3D RECONSTRUCTION OF SIMULATED BRIDGE PIER LOCAL SCOUR USING

GREEN LASER AND HYDROLITE SONAR

by

Musab Banyhany

A Thesis Submitted to the Faculty of

The College of Engineering and Computer Science

in Partial Fulfillment of the Requirements for the Degree of

Master of Science
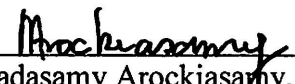
Florida Atlantic University

Boca Raton, FL

May 2018

3D RECONSTRUCTION OF SIMULATED BRIDGE PIER LOCAL SCOUR USING

GREEN LASER AND HYDROLITE SONAR

by

Musab Banyhany

This thesis was prepared under the direction of the candidate's thesis advisor, Dr. Madasamy Arockiasamy, Department of Civil, Environmental and Geomatics Engineering, and has been approved by the members of his supervisory committee. It was submitted to the faculty of the College of Engineering and Computer Science and was accepted in partial fulfillment of the requirements for the degree of Master of Science.

SUPERVISORY COMMITTEE:

_____
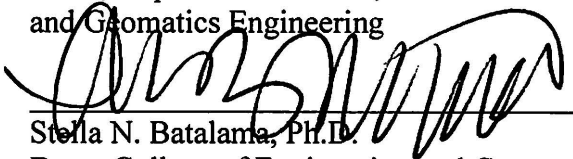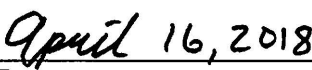Madasamy Arockiasamy, Ph.D., P.E.
Thesis Advisor

_____
Sudhagar Nagarajan, Ph.D.

_____
Khaled Sobhan, Ph.D.

_____
Yan Yong, Ph.D.
Chair, Department of Civil, Environmental and Geomatics Engineering

_____
Stella N. Batalama, Ph.D.
Dean, College of Engineering and Computer Science

_____
Khaled Sobhan, Ph.D.
Interim Dean, Graduate College

April 16, 2018
Date

iii

ACKNOWLEDGMENTS

ABSTRACT

Author: Musab Banyhany

Title: 3D Reconstruction of Simulated Bridge Pier Local Scour Using
                    Green Laser and HydroLite Sonar.

Institution: Florida Atlantic University

Thesis Advisor: Dr. Madasamy Arockiasamy

Degree: Master of Science

Year: 2018

Scour is the process of sediment erosion around bridge piers and abutments due to natural and man-made hydraulic activities. Excessive scour is a critical problem that is typically handled by enforcing design requirements that make the submerged structures more resilient. The purpose of this research is to demonstrate the feasibilities of the Optical-Based Green Laser Scanner and HydroLite Sonar in a laboratory setting to capture the 3D profile of simulated local scour holes. The Green Laser had successfully reconstructed a 3D point-cloud imaging of scour profiles under both dry and clear water conditions. The derived scour topography after applying water refraction correction was compared with the simulated scour hole, and was within 1% of the design dimensions. The elevations at the top and bottom surfaces of the 6.5-inch scour hole were -46.6 and -53.11 inches from the reference line at the origin (0,0,0) of the laser scanner. The HydroLite Sonar recorded hydrographical survey points of the scour's interior surface. The survey points were then processed using MATLAB to obtain a 3D mesh triangulation.

DEDICATION

This thesis manuscript is dedicated to my family, particularly to my inspiring parents, Muhamed and Ludis Banyhany for their love, support, encouragement and sacrifices.

3D RECONSTRUCTION OF SIMULATED BRIDGE PIER LOCAL SCOUR

USING GREEN LASER AND HYDROLITE SONAR

LIST OF TABLES

LIST OF FIGURES

NOMENCLATURE

ρ *and* μ = Fluid density and molecular viscosity respectively

V = Depth averaged velocity of approach flow

y = Approach flow depth

g = Gravity acceleration

Vc = Critical shear velocity for bed sediment entrainment

D and σg = Median size and geometric standard deviation of the foundation material

particle size distribution

ρ_s = Sediment density

c = A parameter describing cohesiveness of the material

b = Pier diameter

Ω = Parameter describing the shape of the pier face (upstream side)

θ = Angle of the flow relative to pier alignment

Z_w = Height difference between the laser scanner and water level

y_s = Scour depth

L_s = Relative scour length (dimensionless)

W_s = Relative scour width (dimensionless)

W = Top width of scour hole

K = Bottom width of scour hole

CHAPTER 1: INTRODUCTION

1.1 BACKGROUND

Scour is a major threat to the safety of waterway bride structures. It is a major factor that impacts the structural integrity and stability of a bridge. It is mainly developed from the process of erosion and sediment transportation around submerged bridge piers or abutments due to hydraulic activities. The hydrostatic forces exerted around a bridge pier cause the riverbed to erode overtime, leading to local scouring. This transportation of soils can be due to several natural and manual factors such as nature of bed materials (e.g. gravel, sandstone, and shales), flooding due to heavy rainfall, sudden increase in the water current due to wind forces, and increased boat traffic. Also, other environmental conditions such as temperature and turbidity of water may alter and increase the rate of scouring process. (Nagarajan, et. al, 2018)

According to the FHWA's National Bridge Inventory (NBI), the total number of bridges categorized as "scour-critical" is 22,900, and approximately 80,000 more bridges are identified as scour susceptible. (NBI, 2017). Natural events such as floods and hurricanes significantly increase the scouring process resulting in millions of dollars in damage to waterway bridge structures. As per Brice Blodgett (1978), the repair cost after every scour event is nearly $100 million to bridge infrastructure. The collapse of a bridge from scour may also cause loss of human life, which has occurred during the Schoharie Creek, Hatchie River, and Arroyo Pasajero River bridge failures (N.T.S.B., 1978; N.T.S.B., 1978).

1

In general, there are three main forms of scour namely general scour, contraction scour and local scour (Prendergast, et. al, 2014). The general scour is usually caused by hydraulic parameters in waterways. Contraction scours are the result of reduced cross-sectional area due to construction of underwater structures. Local scours are formed around individual bridge piers and abutments. In order to minimize the impact of each type of scour, Federal Highway Administration (FHWA) and AASHTO have published various design specifications through Hydraulic Engineering Circulars (HEC).

These HECs include: HEC-18, Evaluating Scour at Bridges (Arneson, et. al, 2012). HEC-23, Bridge Scour and Stream Instability Countermeasures-Experience, Selection, and Design Guidance (Lagasse, 2009) provides guidelines for scour countermeasures. For conducting new or rehabilitation designs for bridges, both HEC-18 and HEC-20 are used. Countermeasure solutions may be developed when there are concerns with regard to scour or stream stability (Hunt, 2005). These guidelines have been continuously revised on modern technology and research. However, approximately 40% of the bridges that are in service today were constructed more than 50 years ago (ASCE, 2017) and redesigning them to meet new guidelines is economically not feasible. Therefore, it is crucial for submerged bridge structures to be monitored regularly to detect potential damages caused by scour.

1.2 RESEARCH OBJECTIVE

The objective of this research is to demonstrate a simulation of local scour around a circular bridge pier using two distinctive methods to measure the geometric profile of the scour. The research is elaborated on two different scour profiles. Each case pertains to a specific scour geometry that was developed using empirical equations for local scour at a single pier structure in cohesionless sediments. The structural size, sediment size,

sediment slope, and inflow depth were all used in the development of the empirical equations based on dimensional analysis. The maximum diameter size of the pier structure that can be tested cannot exceed 15% of the diameter of the circular tank.

1.3 ORGANIZATION OF THE THESIS

This thesis consists of five chapters which detail the essential elements of this research and the work that was undertaken. The literature review in Chapter 2 introduces the reader to the various methods of monitoring the scouring process around bridge piers. This chapter also discusses the feasibility and cost-effectiveness of each existing method for scour evaluation, and the long-term streambed elevation changes that could potentially cause soil displacement around bridge piers. Chapter 3 primarily focuses on the experimental studies on local scour around bridge piers, and the two methods used in the present study based on Green Laser and HydroLite Sonar. The experimental study elaborates on the theory and application of HydroLite Sonar and Leica Green Laser Scanner that were used for scour detection.

Chapter 4 presents the results and discussions based on the Green Laser and HydroLite Sonar methodologies. The data from the HydroLite Sonar instrument are processed to obtain the scour profile in the forms of hydrographs and 3D-mesh triangulations of the topographical points. The data from the Green Laser instrument are processed using Cyclone Software to obtain the 3D reconstruction images of the scour hole under both dry and clear water conditions. Chapter 5 presents an overall summary of the results, and also highlights the differences in the reconstruction of the scour hole. Discussions on the recommendations are given along with a brief description of future research work in the evaluation of bridge pier scour.

CHAPTER 2: LITERATURE REVIEW

2.1 INTRODUCTION

Scouring is the process of sediment erosion around bridge piers and abutments due to natural and man-made hydraulic activities. When the amount of sediment leaving an area is greater than the amount of sediment entering the area, scour occurs. Excessive scouring is a critical problem that is typically handled by enforcing design requirements that make the submerged structures more resilient. The goal of this research is to measure the profile of local scour holes around a bridge pier model using two methods: Green Laser and Hydrolite Sonar.

Bridge owners have adopted various methods to monitor the scouring process and develop retrofitting and rehabilitation measures as needed. One of the existing methods to monitor scour is the visual inspection by divers, which is considered a standard practice. However, the visual inspection is time-consuming, unsafe and not cost-effective. The objective of this study is to develop an experimental procedure to utilize green laser and HydroLite sonar to detect a potential local scour hole and measure the depth and geometry of the scour hole. The green laser technology can be used as a non-contact device and is accurate, fast, and provides high-resolution data. The green laser technology is demonstrated for capturing the scour geometry in a simulated model bridge pier scour hole in a laboratory setup. The scour topography is derived after applying refraction correction and compared with the predetermined scour-hole dimensions as per

4

HEC. The results suggest that the demonstrated green laser based non-contact technique is suitable for scour mapping and monitoring. Instruments for the measurement and monitoring of bridge scour are necessary to study scour processes and to support bridge management. (Xiong Yu, et. al)

The classification of scour detection takes into account function, purpose, measurement technologies, and instrumentation types. Two of the most common categories during the process of detecting potential scour are portable and embedded instrumentation methods. Portable instrumentation is used in diving to take scour measurements during inspection. Ultrasound rods are utilized to transmit beams to the location of the scour. Examples of embedded instrumentation include submerged Radio Frequency (FR) sensors and sonars.

2.2 IMPORTANCE OF STUDY

2.2.1 LOCAL SCOUR AROUND BRIDGE PIERS AND ABUTMENTS

Local scour occurs due to the removal of soil from around bridge piers, abutments, spurs and embankments. It is a gradual process that starts to occur from erosion or an acceleration of hydraulic flow. It is also caused by vortices influenced by obstructions to the flow. Local scour can be classified as either clear-water or live-bed scour.

2.2.2 GENERAL SCOUR

General scour is the downgrading process of the streambed across the stream or waterway bed around bridge piers and abutments. The downgrading may be consistent across the seabed or the scour depth may be deeper in various parts of the cross-section. The contraction of a river flow may result in general scour, which eventually leads to the removal of bed material across the width of the channel. General scour differs from long-

term degradation in the sense that general scour is usually cyclic and may be caused by a flood.

2.2.3 TOTAL SCOUR

Total scour consists of three elements:

1. Long-term aggradation and degradation of the river bed

2. General scour at the bridge

    a. Contraction scour

    b. Other general scour

3. Local scour around bridge piers or abutments

The three elements stated above are summed to determine the total scour at a pier or abutment. These components are meant to be independent of one another and are all incorporated into the design for conservatism.

2.2.4 LONG-TERM STREAMBED ELEVATION CHANGES

When the stream or watershed is altered in such a way that water will flow at a higher rate, this modification causes changes to long-term bed elevation. Therefore, the streambed is either in a state of aggradation, degradation, or in a relative equilibrium. Aggradation is the process in which a river, stream, or current displaces an eroded material. Degradation is the process in which a scour is developed in the streambed due to a shortage in sediment supply from upstream. Long-term aggradation and degradation do not include the cutting and filling of the streambed in the vicinity of the bridge that might occur during a runoff event (general and local scour). An alteration may occur to a long-term trend during the life of a bridge. The alterations of a long-term trend are due to human activities or natural processes. The engineer must know the present state of the stream and watershed

in order to evaluate potential or future changes in the water stream. The engineer must also develop engineering judgment to determine the cause of long-term elevation change.

The main factors that may impact long-term bed elevation changes are dams and reservoirs, watershed transformations, channelization, cutoffs, downstream channel changes, gravel mining from the streambed, diversion of water into or out of the stream, and natural downgrading of the fluvial system.

2.3 SCOUR MONITORING PRACTICE AND TECHNOLOGY

2.3.1 PORTABLE INSTRUMENTATION METHOD

Portable instrumentation methods are based on visual inspections conducted by professional bridge inspectors to monitor potential local scours around bridge piers and abutments. This method serves as an effective way of detecting scour holes and is well suited for bridge maintenance and inspection workers to detect scour conditions around piers and abutments.

2.3.1.1 DIVING

For underwater scour conditions, bridge inspectors dive to inspect the foundation for signs of potential scouring. Scour data from measurements are collected from many locations within the site and the water turbidity does not affect the data collection process. However, this method has a drawback in the sense that this type of inspection can be costly and dangerous. Moreover, the data collected from diving are prone to a high-degree variability due to the subjectivity of the inspectors.

2.3.1.2 SOUNDING RODS OR WEIGHTS

A sounding or falling rod instrument is a manual or mechanical gravity-based physical probe. This instrument is performed by a bridge inspector by releasing a rod or

weight into the streambed to measure the depth of the sediment soil. The bottom of the sounding rod is supposed to be wide in order to prevent penetration of the streambed caused by the weight of the rod. Also, a wide rod at the endcap will prevent penetration caused by vibration that is due to water flow. One drawback of utilizing a sounding rod is the inaccuracy of the data samples attained and the potential danger a bridge inspector may encounter. This method can be quite expensive and is not subjected to automated alerts.

2.4 EMBEDDED INTRUMENTATION METHOD

2.4.1 OVERVIEW

Embedded instruments are used as sensors submerged underwater to monitor scours around bridge piers. These sensors are usually mounted in a fixed position on bridge piers and are activated once the scour is in the process of being developed. Once these sensors start to record data, they send wave signals to alert the safety personnel of potential scouring. The most common embedded instruments are sonar-based sensors, magnetic sliding collars, float-out devices, tilt meters, and sounding rods. Embedded sensors tend to record data of scour depth in the vicinity of the area where they are installed and mounted. The advantage of this method is that it does not require bridge inspectors to be present on site.

2.4.2 SONARS

Sonar is a system that is utilized for the detection of objects underwater and measuring the depth of water. When sonar is submerged underwater, it will take measurements by emitting sound pulses and measuring their return after being reflected. Sound travels much faster and have less dissipation in water than air. Therefore, echo sounders with single or multi-beam capability have been widely used.

2.4.2.1 SONAR-BASED SENSOR METHOD

Sonar-based sensors are instruments installed in a fixed position and are typically mounted on the surface of a pier or abutment. The sonar is connected to a transducer via serial cable and the transducer functions by emitting a sound pulse wave to the waterbed. During the wave transmission, the sonar calculates the round-trip travel time of a pulse at the streambed to measure the depth and surrounding slopes of scour. Sonar sensors have the advantage of measuring not only the scour depth, but the deposition of sediments as well. The downfall of sonar sensor applications is that the readings may be affected by turbidity and turbulent flow. High-end sonars with high depth capacity and resolution can be extremely expensive.
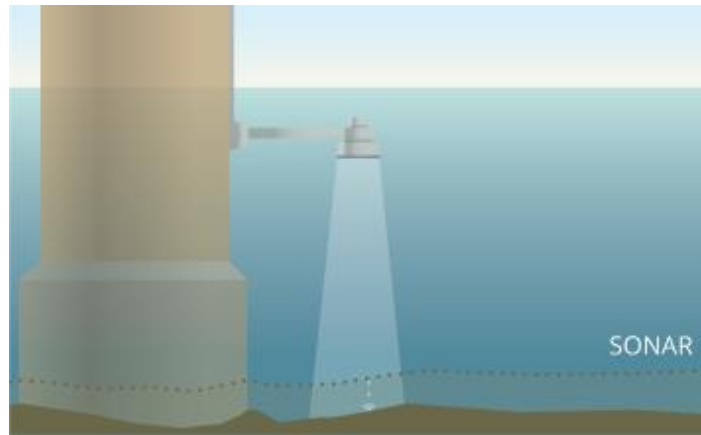
Figure 1: Sonar-Based Sensor Mounted on a Bridge Pier

2.4.3 TIME DOMAIN REFLECTOMETER (TDR) METHOD

The Time Domain Reflectometer (TDR) method is similar to a sonar-based sensor to measure scour. The only difference is that the magnetic sound pulse in a TDR is transferred through sensor conduits. The benefit of the magnetic pulse is it has the capability of determining the portion of the conduits buried in the streambed. Another advantage is that it is capable of conducting survey tests in a repetitive manner. This technique, however, requires an abundant amount of power, which makes the process expensive. The signal analysis instrument that is compatible with the Time Domain Reflectometer (TDR) is sometimes difficult to calibrate. Figure 2.4.3 illustrates a schematic of a scour monitoring system using TDR probes to transfer collected data through conduit tubes.
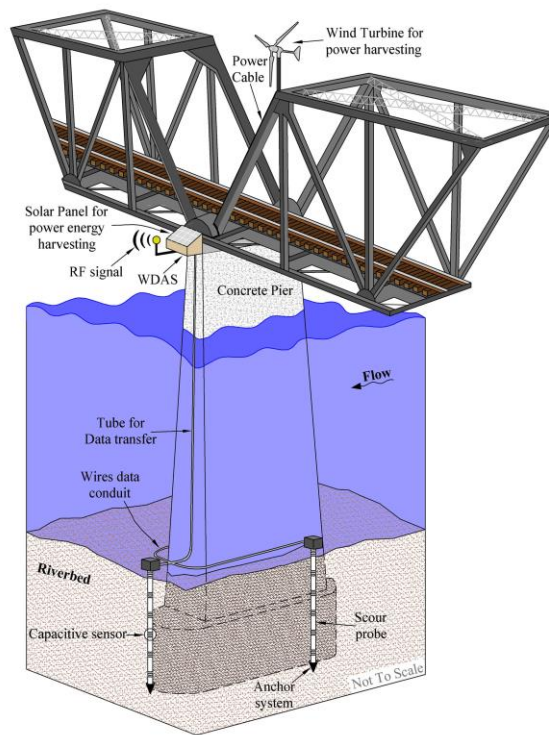
Figure 2: TDR Bridge Scour Monitoring System Schematic

2.4.4 TILT-METER METHOD

Tilt-meters, also known as inclinometers, is mainly designed to monitor and measure the depth of local scour around a bridge pier or an abutment from a vertical level. It is usually mounted to a bridge pier structure. When the structure tilts or starts to sway due to scour, the tilt-meters will sense this change and eventually begin to measure the scour and deposition of sediments. Relatively, this technique is quite feasible and highly preferable for extreme local scour cases. Figure 3 illustrates a fixed tilt-meter that is mounted on the cap of a bridge pier.

Figure 3: Tilt-Meter Sensor Mounted on a Bridge Pier

2.5 RADAR OR PULSE SENSORS

Pulse or radar devices are used to generate radar signals or electromagnetic pulses to find particular alterations in the material properties that develop when a signal is propagated through a changing physical medium (Forde et al., 1999). These devices function when a radio signal is transmitted using a probe that is made in the scour region. These devices are similar to the single-use devices in the sense that they are very expensive to install, to acquire one sample of scour depth. Another version of radar devices utilizes

11

Ground Penetrating Radar (GPR) on the water surface. The detection of scour depth is dependent on the multiple-return of the transmitted electromagnetic radiation. Just like the latter devices, GPR is expensive and bulky. Also, mapping seabed results in noisy radar returns.

2.5.1 MAGNETIC SLIDING COLLAR METHOD

A magnetic sliding collar is a very useful and effective device that aids in detecting potential local scour. This device consists of stainless steel pipe that is driven into the bottom of the channel with a sliding collar. The sliding collar drops down the pipe as the scour progresses. When soil erodes around a bridge pier, the collar slides downs the magnetic rod with a decrease in level. The base station at the bridge will detect a change in the collar's height and will send signal messages to the designated officials. The main drawback of this instrument does not measure soil sediment deposition.
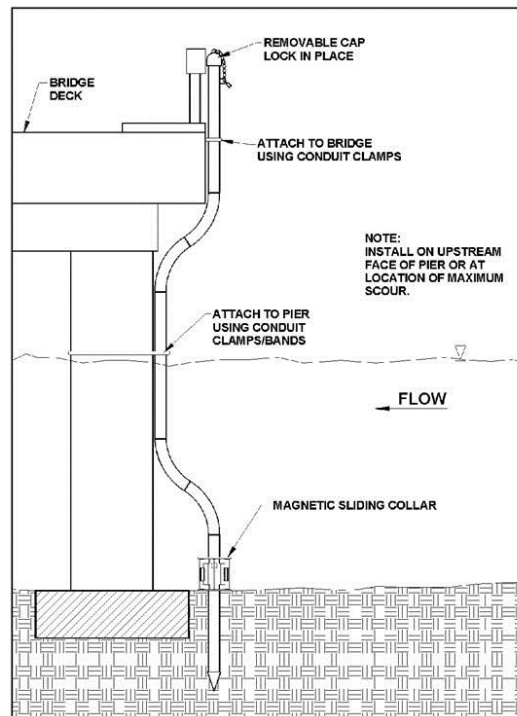
Figure 4: Embedded Magnetic Sliding Collar Schematic

2.6 VIBRATION-BASED METHOD

The vibration-based method is used to measure the frequency of a rod that is embedded in the streambed. This technique has structural vibration sensors such as accelerometers or Fiber-Optic Bragg-Grating (FBG) to use as a dynamic sensing element of the scour sensor. However, vibration-based sensors are currently being tested in labs and are not in practice for real-world applications.

2.7 ACOUSTIC DOPPLER CURRENT PROFILER METHOD

An acoustic Doppler current profiler (ADCP) is a hydroacoustic current meter used to measure water current velocity profile at the bridge pier location. The water current velocity is measured over a certain depth range by the use of the Doppler effect of sound waves being scattered back from particles within the water column. This technique aids in scour forecasting. An Acoustic Doppler monitors the scour indirectly because it only determines the depth at which the water is flowing and the velocity profile over a period of time. This instrument is not feasible under snow and ice conditions. Figure 5 illustrates a fixed Acoustic Doppler instrument that is mounted on the bridge deck and submerged underwater. The distributed diagram in the figure represents the velocity at which the channel is flowing. The surface velocity is computed by radar sensors embedded in the instrument. The velocity and cross-sectional area of the water column are multiplied to obtain the discharge.
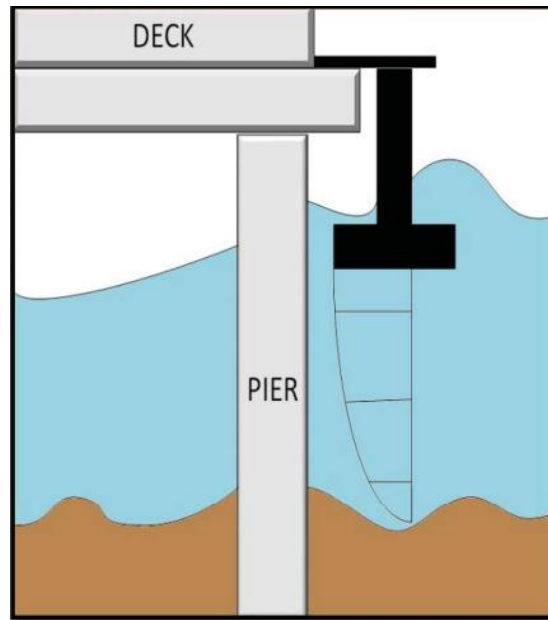
Figure 5: Acoustic Doppler

2.8 SUBSURFACE GEOPHYSICAL METHOD

Subsurface geophysical instruments are used to measure the physical properties of the subsurface. These instruments combine on-going seismic reflection profiling with ground penetrating radar. This technique has the ability of providing accurate results and is capable of conducting real-time scour measurements. This instrument, however, is very expensive to install and is difficult to use. It requires an expertise to analyze the data collection. It is hard to automate and is not effective in deep water. Geophysical instruments are mainly used after flood hazards during low flow conditions to measure potential scour holes and areas of infilling.

2.8.1 ACCELEROMETER

The accelerometer is an instrument used to measure the acceleration of the structural member that is attached to it. It is used for measurements of vibration properties, which are usually caused by the change in support conditions of the bridge. The vibrations

of the bridge structure in this case is due to local scour at the pier or abutment. Accelerometers are easy to install and maintain but they require excessive amount of power to transmit and for post-processing. Figure 6 shows an accelerometer sensor mounted on a bridge pier and is activated to sense a vibration in the bridge due to local scouring.
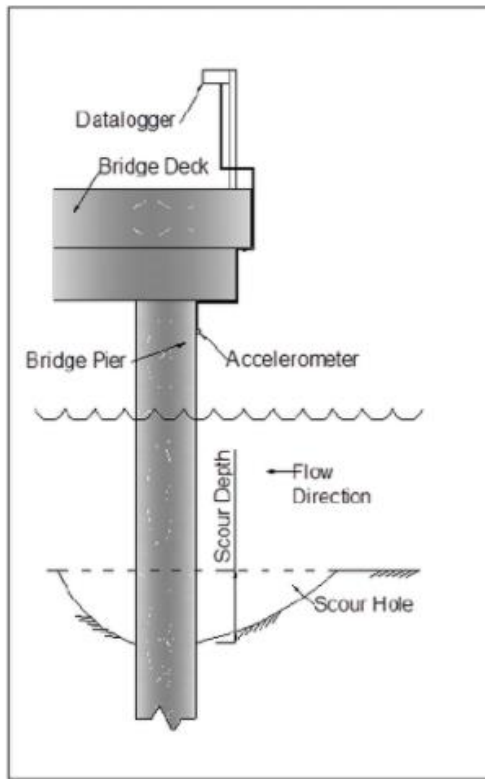
Figure 6: Accelerometer Mounted on the Bridge Pier

2.9 SINGLE-USE DEVICES: BURIED RF SENSOR

Single-use devices are simple mechanical devices installed vertically near a pier or abutment. When the scour develops, the devices will no longer be stable vertically and start to float. The purpose of these devices is to activate and send signals to the data collection system when it starts to float. The signal that is sent to the data collection system would eventually inform the safety personnel of scouring process (Briaud, et. al, 2011). This

device however, has a very high installation cost to detect scour at one sample point. This drawback affects the ability to measure the overall geometry of the scour.
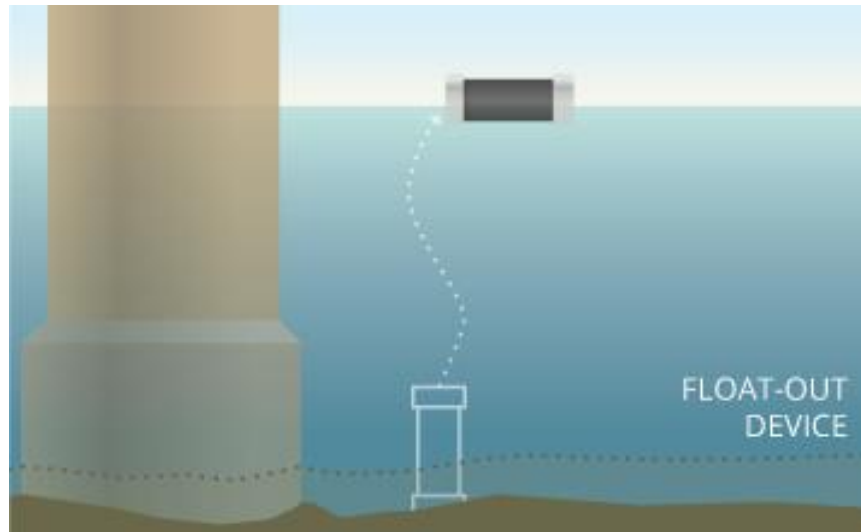
Figure 7: Buried RF Sensor

2.10 GRAVITY SENSORS

Gravity sensors are devices that can measure the gravitational acceleration. They can detect changes in orientation. Gravity sensors are utilized to monitor the scour when sediments are relocated or eroded from the bridge pier. The sensors are embedded in the piers and abutment and stabilized on the streambed around local scour critical regions. Overtime, as scour progresses, the streambed will eventually erode and the sensors will initiate, conducting various gravity measurements due to the displacement of mass (Prendergast, et. al, 2014). Another purpose of embedding gravity sensors is to measure scour depths and slopes only at the location at which the gravity sensor is installed. The fact that it only measures from its location, this limits the measurement of the overall shape of scour.

2.11 PHOTOGRAMMETRY

Photogrammetry has been widely used to for scour mapping in clear water conditions. It is the method that uses an abundance of images taken from different locations to simulate a 3D model. (Umeda et. al, 2010) uses a non-uniform cylindrical pier in laboratory environments to study the scour under simulated stream flow. (Reike-Zapp et al, 2005) used close-range photogrammetric techniques to measure the dimensions of soil erosion with mm level precision. The authors use a laboratory experiment to develop the methodology that measures the volume underwater sediment transportation. (Heng et. al, 2010) also use similar approach to study soil erosion using photogrammetry.

There are certain limits in the existing scour monitoring methods to provide enough number of samples on the scour surface with less cost, labor, and time. The accurate mapping of scour is crucial to understanding the immediate, near-future and long-term implications on the structural stability of submerged structures. Therefore, this research demonstrates a non-contact, green laser based ranging technique that can provide accurate representation of the scour by sampling it with thousands of points in a few seconds. The details of the proposed technology and relevant mathematical model are discussed in *Chapter 3: Experimental Study on Bridge Pier Scour.*

CHAPTER 3: EXPERIMENTAL STUDY ON BRIDGE PIER SCOUR

The present study uses a sonar-based HydroLite-TM and an optical laser-based instrumentation that emanates green laser for mapping the idealized scour profile in a model bridge pier. The theory for the HydroLite and Green Laser are presented in the following section.

3.1 THEORY AND APPLICATION OF HYDROLITE SONAR SCOUR DETECTION

The HydroLite-TM is a portable, integrated bathymetric survey system that is designed as a turnkey, shallow water single-beam rig. The Survey Pole Kit comes in a rugged carry case shown in Figure 8 and provides an integrated survey solution for shallow water conditions.

Figure 8: HydroLite-TM in rugged carry case

In this research, the main purpose of the application of HydroLite Sonar is to map the streambed and detect local scour around a bridge pier. The hydrographic survey will demonstrate the depth of local scour and the slope from all sides of the scour. The application is further explained in the Methodology chapter. The HydroLite-TM consists of 2-foot survey pole section (1-1/4-inch diameter pole), a GPS antenna that is mounted over of the pole, a SonarMite echosounder that is mounted on the pole, a transom mount to stabilize the pole onto a boat, a pole transducer mounting bracket (universal boat mount), and a survey point. The Hydrolite-TM schematic is illustrated in Figure 9.
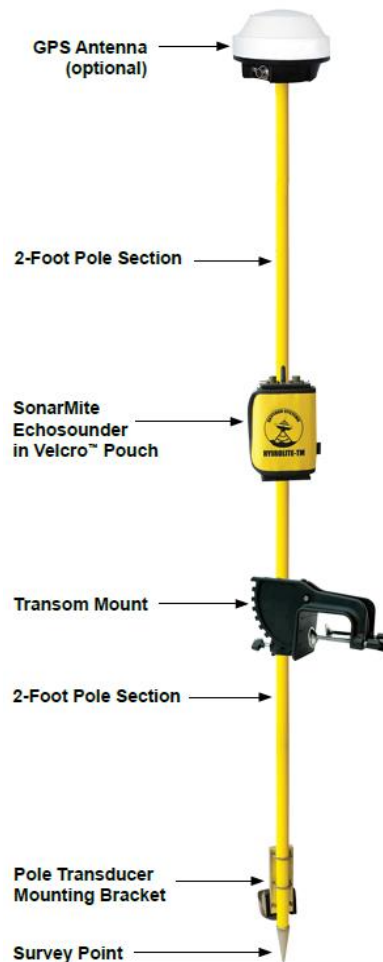
Figure 9: HydroLite-TM Schematic

3.1.1 SONARMITE MILSPEC BLUETOOTH ECHOSOUNDER

The SonarMite Echosounder is a Bluetooth Portable Survey System that combines low and high frequency transducers in one unit, and is primarily used for shallow water hydrographic surveying. The Echosounder's battery is rechargeable and can last up to 12 hours. The simplicity of the Echosounder is that it is utilized without buttons and is splash proof. Between the low and high frequency is a residual difference that is mainly visible on an echogram. This residual difference expresses the fact that the thickness of mud in the soft sediment layer can be measured. When mud thickness is measured, the surveyor must use particular equipment that is mainly designed for geophysical measurements. Geophysical measurements could be a sub-bottom profiler, seismograph, a penetrator or a bottom sample.

This SonarMite Echosounder instrument enables penetration through soft sediments to detect harder layers and functions as a tool for bottom classification. It is easily mounted on the survey pole as shown in Figure 9 and contains an internal battery, Bluetooth system to retrieve data from the Echosounder, IP65 weatherproofing, and MILSpec connectors and caps. The Echosounder becomes active and ready to use when the transducer shell at the bottom of the survey pole is connected to the SonarMite MILSpec Echosounder via serial cable. The top-view of the Echosounder connectors is shown in Figure 10.

Figure 10: SonarMite MILSpec Echosounder connectors

The SonarMite Echosounder has 2 connectors; the XDR and PC connector. As shown in Figure 10, the transducer cable is connected to the XDR connector. The PC connector is for connecting to a PC or data collector to obtain survey points of bottom elevation.

The SonarMite MILSpec Echosounder is utilized for multiple elements as follows:

- Log into HYPACK or other hydrographic survey software on laptops

- Using Differential GPS: to provide positional corrections to GPS signals

- Real Time Kinematic (RTK) GPS: used for satellite navigation as a technique to achieve accurate data from satellite-based positioning systems

- Survey Topo software on data collectors

- SM Mobile software

- Remotely controlled unmanned boats

- Robotic total stations

3.1.2 HYDROLITE-TM ECHOSOUNDER TRANSDUCER

The Echosounder transducer is a digital smart instrument with a frequency of 200 kiloHertz that is mounted to the bracket at bottom of the survey pole as shown in Figure 9. The transducer-mounting bracket will accommodate the survey pole when submerged under water for a hydrographic survey. The transducer shell has a 10-foot long transducer cable that connects to the SonarMite Echosounder in order for the Bluetooth system to function properly.

The height of the survey pole is 2 feet and is given as input to the data collector before starting the survey. The transducer will measure the depth below the transducer shell and is applied to the rod offset as input to the data collector. As the survey pole moves from point to point, it will log bottom elevation to the data collector. The narrow beam that is emitted from the transducer is typically presented as a radial distribution pattern versus output power applied. In other words, the beam width of the transmitted ultrasound increases with amplitude. Moot modern Echosounders has a processed digital signal method to lessen the power or gain of its transmitted signal. Hence, this technique maintains the width of the beam for a given transducer.

The advantage of utilizing a transducer to transmit a narrow beam width is the ability to visualize narrow valley shapes to gain a high-resolution representative definition of the bottom elevation that is surveyed throughout. After the ultrasound transmission hits the seabed, the returned signal within the ultrasound beam is the shallowest point within the beam.

3.1.3 LEICA DATA COLLECOTR

The data collector is a Leica Geosystem Viva CS15 controller that is connected to the SonarMite Echosounder by serial cable or Bluetooth. The controller used for the research experiment to log topo data points is shown in Figure 11.

Figure 11: Lieca Viva Controller Data Collector

3.1.4 LEICA VIVA GS14 ANTENNA

The Leica Viva GS14 antenna is powerful and is capable of measuring any task with integrated mobile communications and UHF modem. The antenna is a smart GNSS instrument that has reliable features and gives accurate data. The purpose of the smart antenna is to receive and amplify radio signals being transmitted on high frequency waves by GPS satellites. These radio signals are converted to an electronic signal to compute data during a hydrographic survey. The GNSS smart antenna is shown in Figure 9.

3.2 THEORY AND APPLICATION OF GREEN LASER SCOUR DETECTION

3.2.1 INTRODUCTION

Terrestrial Laser Scanners (TLSs) are laser ranging based 3D geometric devices that capture data and produce high-resolution sampling of the scene in a short period of time. It is mainly used for non-contact or targetless operations. The TLS functions on the rule of ranging which inputs the coordinates of objects or surface in the region by using its distance from the laser scanner and laser pulse orientation. The distance between the scanner and the object is measured using time-of-flight or phase shift methods. The time-of-flight technique provides the range based on a specific time length between transmitted and received laser pulse and speed of the pulse. Another technique known as the phase-shift method develops the range by inputting the number of full and partial waves that is set in between the time it is sent and received. The origin of the eye of the laser scanner in the coordinate system is (0,0,0). The laser ray that is emitted from the laser scanner is given by the horizontal angle *(θ)* known as the azimuth and vertical angle *(φ)*. From the path of the laser pulse, the observed range determines the coordinate of the point in 3D space. The 3D Cartesian coordinate system is illustrated in Figure 12.
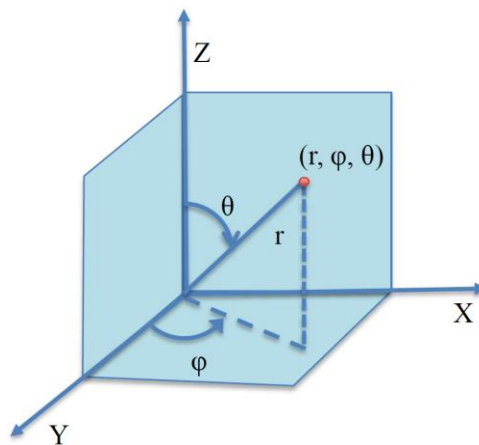
Figure 12: Polar to 3D Cartesian Coordinates

24

Where,

$$X = r \, sin\varphi \, sin\theta$$

$$Y = r \, sin\varphi \, cos\theta$$

$$Z = r \, cos\varphi$$

The majority of laser scanners use either infrared or green wavelength lasers. The spectral properties of water cause infrared wave lasers to be completely absorbed, hence reflection or scattering is not produced. This research demonstrates a methodology to utilize green laser for underwater scour monitoring. Green laser with wavelength of about 500 nm can penetrate through the water surface and hit the seabed/riverbed of the waterbody and reflect back to the receiver (laser scanner). By this process, the laser pulse travels through multiple mediums and make several interactions with the surface. When laser is transmitted from the scanner, it travels from the air medium to water, causing refraction to occur on the refraction plane and reaches the bed of the waterbody. Then the laser pulse typically goes through a diffuse scattering (i.e scattering in all directions). The scattered or reflected pulse in the angle equal to the incident angle reaches the receiver located at the laser scanner. The geometry of this ranging principle is shown in Figure 12. The figure is modified from Smith et al [20] and Plennar [21].

3.2.2 LASER-BASED OPTICAL APPROACH

The laser-based optical approach utilizes a green laser to conduct a 3D scan of the surrounding area. Green laser has been widely used for bathymetric applications by mapping community through airborne missions. However, such laser scanning systems are bulky, expensive, less dense and not suitable for local scour mapping. Green laser is a very useful instrument for close-range mapping and has been used for various hydrologic and

sediment mapping applications. Hodge et all [22] utilized green laser to map fluvial sediment surfaces.

Smith et al [20] used green laser to attain high-resolution structure and particle size data for gravel beds to understand the interaction of bed roughness with near-bed flow hydraulics, sediment entertainment, transport and deposition. Miura and Asano [23] predicted sediment flow using green laser for disaster risk management in waterways at mountains. Smith et al [20] and Plennar [21] developed a mathematical model using green laser to map hydraulic and fluvial environments. In addition, the paper also discusses the applications of these techniques for scour risk modeling and stream-bank retreat monitoring.

3.2.2.1 LEICA SCANSTAION II GREEN LASER

Leica ScanStation II is a green laser instrument used for high-definition surveying to collect timely, accurate and complete geometric data of existing sites and structures. In this research, the ScanStation II instrument will be used to scan a 3D model of an existing scour hole around a bridge pier. The present study involves as a laboratory experiment on a model bridge pier local scour measurement using Leica ScanStation II. Figure 13 illustrates Leica ScanStation II that is mounted on a tripod, along with cables connected to a laptop. The scanner at the top of the ScanStation emits a green laser that scans the surrounding area, forming a 3D model of the area in Cyclone software. The laptop shown in the figure contains Cyclone software which is needed to collect 3D data of the scanned area.
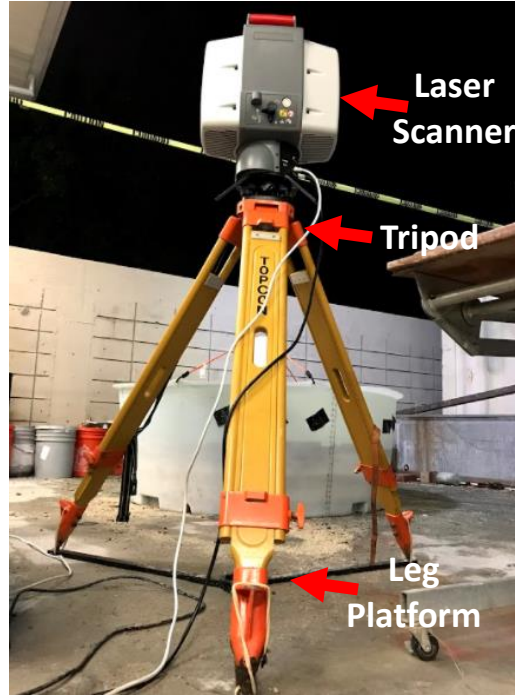
Figure 13: Green Laser Scan Station II mounted on a Tripod

In the laboratory conditions, the ScanStation will transmit the laser from the scanner into the waterbed to scan the submerged scour hole. The laser transmission underwater causes a refraction to occur. Smith et al [20] derived equations for underwater scanning and refraction correction. When the laser is transmitted from the origin of the laser scanner, it travels in the air medium to the water level and refracts through the water surface. Snell's law satisfies this process of refraction. The ratio of sines of the incident angle (θ_a) in air and the refracted angle (θ_w) in water is given by the inverse of their refractive indices. The refractive index is the ratio of light velocity in a vacuum to its velocity in a specified medium. Generally, the refractive index of air and water is assumed to be 1 and 1.33538 respectively (Daimon, et. al, 2007). Snell's law is given below and was adapted from [20-21].

$$\frac{sin\theta_a}{sin\theta_w} = \frac{1.33}{1}$$

When green laser is used to scan submerged surfaces without refraction correction, the laser scanner will assume the laser pulse has not refracted. It will rather place the point *(X,Y,Z)* in a straight line along the angle of incidence, which is farther from the location the laser is reflected from. This assumes the laser emanates from the coordinates (0,0,0) with offsets in *X,Y* and *Z* directions being removed using the method demonstrated in [20]. The farther distance placement is due to the assumption by the laser scanner that the medium is simply air throughout. However, the return laser pulse would have refracted through the water at the angle θ_w and hit the waterbed at the point (X_r, Y_r, Z_r). Since water has a higher refractive index, it would travel a shorter range than the uncorrected point with coordinates of *(X,Y,Z)*. The coordinates of the point where the laser hits the water surface is denoted as (X_w, Y_w, Z_w). Since the laser does not provide the angle of incidence explicitly, it can be computed using uncorrected horizontal range *(R)* and *Z (Z)* coordinates. Hence,

$$\theta_a = tan^{-1}\frac{R}{Z}$$

Where,

$$R = \sqrt{X^2 + Y^2}$$

By using Snell's equation, the angle of reflection (θ_w) can be computed as,

$$\theta_w = sin^{-1}\frac{sin\theta_a}{1.33}$$

The horizontal distance from the laser to the water surface (R_w) is obtained by,

$$R_W = Z_w * tan\theta_a$$

The variable (Z_w) is the height difference between the laser scanner and the water level.

Similarly,

$$R = Z * tan\theta_a$$

The refraction angle θ_w equation is given by,

$$\theta_w = tan^{-1}\frac{R_r + R_w}{Z_r + Z_w}$$

Equation 5, 6, and 8 will lead to the following formula shown below:

$$Z_r = \frac{1.33 * cos\theta_w(R_r - R_w)}{sin\theta_a} + Z_w$$

Where,

$$R_r = \frac{R - R_w}{1.33^2} + R_w$$

The azimuth of the laser pulse ($\emptyset_w$) can be calculated using the equation provided below:

$$\emptyset_w = tan^{-1}\frac{X}{Y}$$

After applying the refraction correction, the *X, Y,* and *Z* coordinates are given by,

$$X_r = R_r sin\emptyset_w$$

$$Y_r = R_r cos\emptyset_w$$

This method requires the height of the water surface (Z_w).
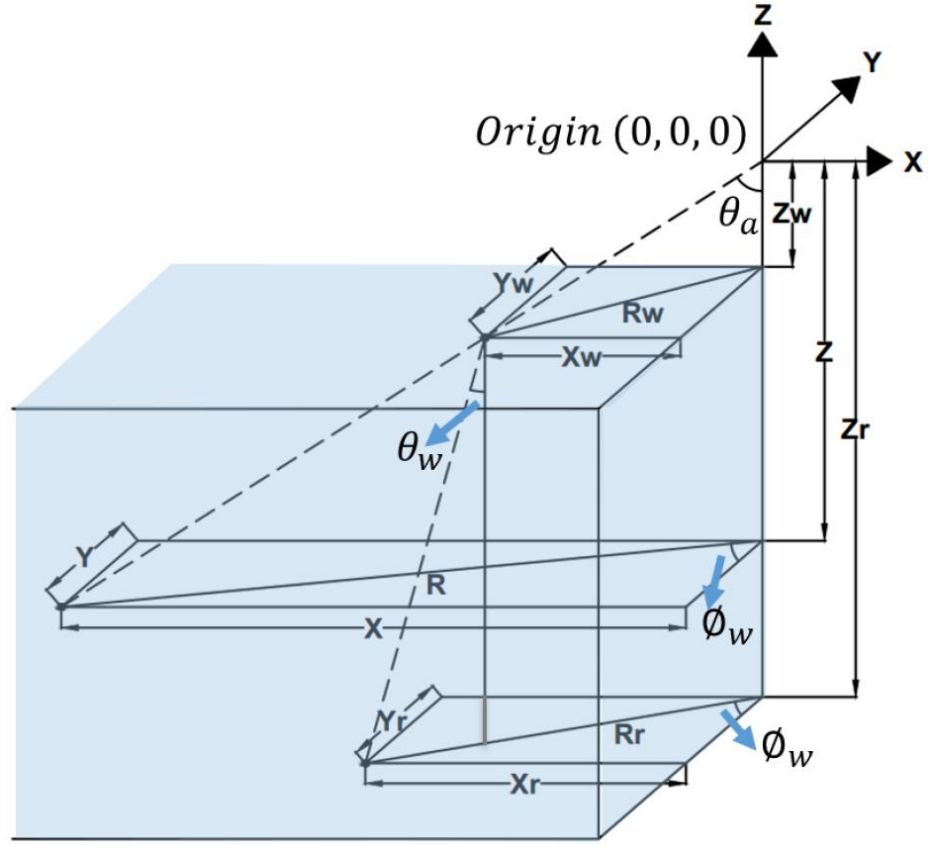
Figure 14: Schematic Representation of Applying Refraction Correction

3.3 METHODOLOGY AND SIMULATION OF LOCAL BRIDGE PIER SCOUR

The cylindrical pier in a single foundation stratum was based on the extensive published literature on pier scour at a cylindrical pier in a single stratum of non-cohesive foundation material; the basic variables are identified and shown in Figure 15. The functional relation between the depth of local scour, y_s, and the variables can be stated as

$$y_s = function \; [flow(\rho, \mu, V, y, g), bed \; material \; (D, \sigma_g, \rho_s, V_c), pier \; (a, b, \Omega, \boldsymbol{\theta}), time$$

Where,

$\rho \; and \; \mu$ = Fluid density and molecular viscosity respectively; V = depth averaged velocity of approach flow; y = approach flow depth; and g = gravity acceleration; V_c = critical shear

velocity for bed sediment entrainment; D and σ_g= median size and geometric standard deviation of the foundation material particle size distribution; ρ_s = sediment density; and c = a parameter describing cohesiveness of the material; a = pier width; b = pier diameter; Ω = parameter describing the shape of the pier's face (upstream velocity); θ = angle of the flow relative to pier alignment; and t = time.
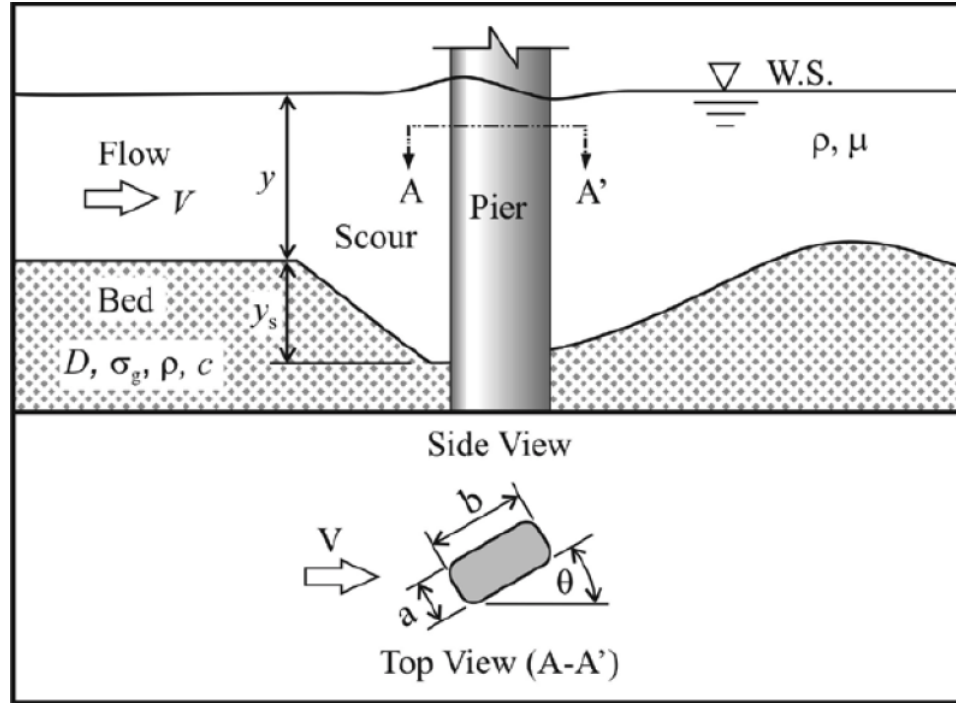
Figure 15: Variables influencing pier scour at a cylindrical pier [25]

Local Pier Scour Prediction: The equation used by Richardson et el. 2001 [26] for estimating the depth of local scour at piers account for additional parameter influences [27-28] is given by

$$\frac{y_s}{a} = 2.0K_1K_2K_3\left\{\frac{y}{a}\right\}^{0.35} Fr^{0.43}$$

where, $Fr = V/(gy)0.5$; and K_1, K_2, and K_3 represent the adjustment factors accounting for the pier nose shape, angle of attack of flow, and state of bed-sediment motion, respectively.

The factor K_1 varies between 0.9 and 1.1, K_2 varies between 1.0 and 5.0 and K_3 varies between 1.1 and 1.3. The top width of the scour hole in cohesionless bed material from one side of a pier or footing can be estimated from the following equation (Khwairakpam, et. al, 2012):

$$W = y_s(K + cot\theta)$$

In the formula equated above, the variable "W" represents the top width of the scour hole from each side of the pier or footing, m. The variable "y_s" represents the scour depth, "K" represents the bottom width of the scour hole, which is related to the depth of scour. The variable "θ" is the angle of repose of the bed material ranging from roughly $30°$ to $44°$. The angle of response of cohesionless material in air ranges from about $30°$ to $44°$. Therefore, if the bottom width of the scour hole is equal to the depth of scour y_s (K=1), the top width in cohesionless sand would vary from 2.07 to 2.80 y_s. At the other extreme, if K is equal to zero, the top width would then vary from 1.07 to $1.8y_s$. Thus, the top width could range from 1.0 to 2.8 y_s. A top width of 2.0 y_s is subjected for practical applications. Length of Scour Hole: As per dimensional analysis, scour length (L_s) is a function of densimetric Froude number and inflow depth. Linear trend lines for the relative scour lengths of different inflow depths are assumed in the following form:

$$L_S = C_2 D_S + D_2$$

Where, C_2 and D_2 are constants dependent on inflow depths. Relative scour length (Richardson, et. al, 2001) is given by:

$$L_s = \left\{3.958\left(\frac{h}{b}\right) - 2.371\right\}D_2 + \left\{-2.649\left(\frac{h}{b}\right) + 5.082\right\}$$

Wherein, h = approach flow depth, b = pier diameter and D_2 = relative depth (local equilibrium scour depth/pier diameter). The relative scour width (Richardson, et. al, 2001) is given by

$$W_s = \left\{ 6.204 \left(\frac{h}{b} \right) - 5.412 \right\} D_2 + \left\{ -4.435 \left(\frac{h}{b} \right) + 7.597 \right\}$$

The scour geometry is computed based on the following parameters:

Local scour depth (d_s) = 8.5 inches = 0.216 meters (m)

Inflow depths = 0.07 m

Average inflow depth (h) = 0.07 m

Pier diameter = 0.168m

Simulated scour width and length are computed using Eqns. 16 and 18 and the longitudinal and transverse cross-sectional views of the scour hole are shown in Figure 20 shows the experimental schematic of the bridge pier scour hole.

3.4 EXPERIMENTAL SETUP

The experimental work was conducted in the Civil Engineering Materials Laboratory at Florida Atlantic University. This study presents a series of experiments to measure the scour profile under dry and clear water condition on cohesionless bed material. A rounded open-top tank is used to form a soil stratum made up of pebbles and cohesionless paver sand. A 6.6-inch circular pipe is installed at the center of the tank simulating a bridge pier with full embedment depth into the soil strata. The tank has a total volume of 10,129 in^3 and has a maximum capacity of 280 gallons. The height of the 280-gal tank is 24 inches and has an inner diameter of 63.5 inches from the top and a diameter of 57.5 inches at the base. The first step of the setup was to clean the tank from dust by spraying water all around it. A total of 12 bags of pebbles were brought to the lab to fill the base of the tank up to a

height of 3.5 inches, as shown in Figure 16. Each bag of pebbles has a volume of 0.5 ft^3, so the total volume of pebbles needed to fill the base is about 5.8 ft^3. The bags were opened and all pebbles were spread evenly on a plastic sheet to be sprayed by a water hose to remove dirt and dust, as illustrated in Figure 17.

Figure 17: Vigoro 0.5 cu. ft. River Pebbles

Figure 16: Washed Pebbles

After the pebbles were cleaned and dried, they were shoveled into the tank. A 6-inch PVC pipe with a height of 3 feet was used as a pile and was placed through the pebbles

and in the center of the tank as shown in Figure 18. The outer diameter of the PVC pipe is 6.625 inches. A pile of concrete was placed inside of the hollow circular pile to stabilize it in the center. The exposed surface was marked along the height at increments of 1 inch for visual observation of the scour profile.

Figure 18: Graduated Pile with Pebbles at a depth of 3.5"

3.4.2 SCOUR SETUP

The idealized scour dimensions were developed using the derived empirical formulas from section 3.3. The scour models are categorized into 2 case studies: Case study I will have a scour depth of 8.5 inches and case study II will have a scour depth of 6.5 inches. These scour models were placed around the pile one at a time to simulate the scour geometry in a riverbed.

3.4.2.1 CASE STUDY I

Case study I presents the setup of a 3-D concave scour model with a known, maximum depth of 8.5 inches. The scour hole depth dimensions were determined from the derived empirical equations. The scour depth and the average inflow depth values were needed to compute the equations stated in *3.3 Methodology And Simulation Of Local*

Bridge Pier Scour Hole. A scour depth of 8.5 inches and an average inflow depth of 2.756 inches were incorporated into the equations. Firstly, the relative scour depth was calculated as follows:

$$D_s = \frac{d_s}{b}$$

Where

D_s = Relative scour depth (dimensionless)

d_s = Scour depth = 8.5" (0.216 m)

b = Pile diameter = 6.625" (0.168 m)

$$D_s = \frac{d_s}{b} = \frac{0.2159 \ m}{0.168 \ m} = 1.28$$

Next, empirical equation 18 was used to calculate the relative scour length of the top surface, L_s, as shown below:

$$L_s = \left\{ 3.958 \left(\frac{0.07 \ m}{0.168 \ m} \right) - 2.371 \right\} (1.28) + \left\{ -2.649 \left(\frac{0.07 \ m}{0.168 \ m} \right) + 5.082 \right\}$$

$$= 3.054 \ m/m$$

The relative scour length was used to compute the scour length, l_s, as shown below:

$$l_s = L_s b = 3.054 * 0.168 = 0.513 \ m = 20.197 \ inches$$

The relative scour width of the top surface, W_s , is calculated using equation 19 as follows:

$$W_s = \left\{ 6.204 \left(\frac{0.07 \ m}{0.168 \ m} \right) - 5.412 \right\} (1.28) + \left\{ -4.435 \left(\frac{0.07 \ m}{0.168 \ m} \right) + 7.597 \right\} = 2.13 \ m/m$$

The relative scour width was used to compute the scour width, w_s , as shown below:

$$w_s = W_s b = 2.13 * 0.168 = 0.357 \ m = 14.05 \ inches$$

For the bottom surface of the scour model, the known length and width were 9.25 inches and 7 inches respectively. The plan view of the scour model is seen in Figure 19.
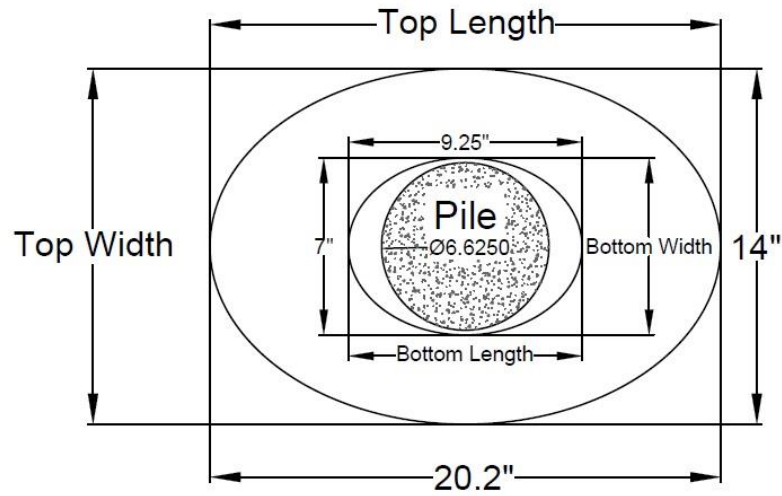
Figure 19: Plan view of the scour model

The longitudinal and transverse cross-sectional views of the scour hole are shown in Figure 20. For the longitudinal and transversal cross sections, their angles of repose of cohesionless material did not fall in the range of 30° to 44°. Rather, the angle of repose at the longitudinal and transversal cross sections were 57° to 69° respectively. Figure 20 also shows the schematic of the bridge pier scour hole.

(a)   (b)
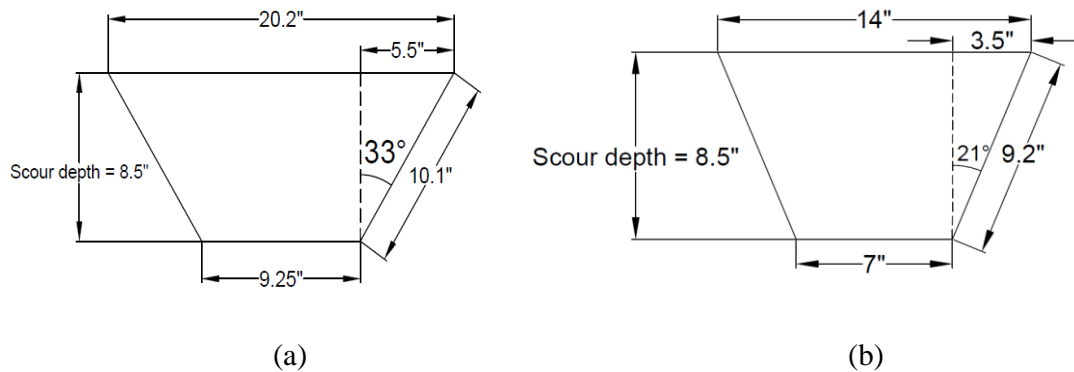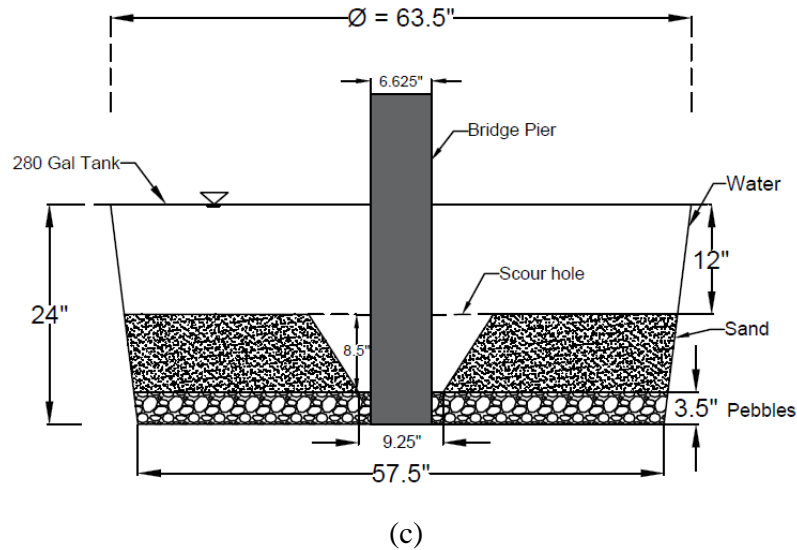
Figure 20: (a) Longitudinal cross section; (b) Transverse cross section; (c) Experimental Schematic of Simulated Bridge Pier Scour Hole

In the experimental schematic of the simulated bridge pier local scour, the bottom layer of the streambed consists of one layer of coarse 3.5 in. river pebbles overlain by 8.5 in. fine cohesionless sand layer. The displaced bed material shown in the schematic will have a scour model of known dimensions embedded around it. The purpose of the scour model is to hold the steep slopes of sediment in place, keeping the area compacted and undisturbed. The scour model will also prevent the waterbed on top of the soil profile from disturbing the displaced bed material.

After using the empirical equations to determine the dimensions of the scour model and angles of repose, a 2-D plan of the scour hole was drawn to scale on a poster. The plan contains the layout of the oval-shaped surface along with the dimensions. The first step was to draw 2 ovals via compass and combine them into one whole oval of known dimensions. The layout is illustrated in Figure 21.
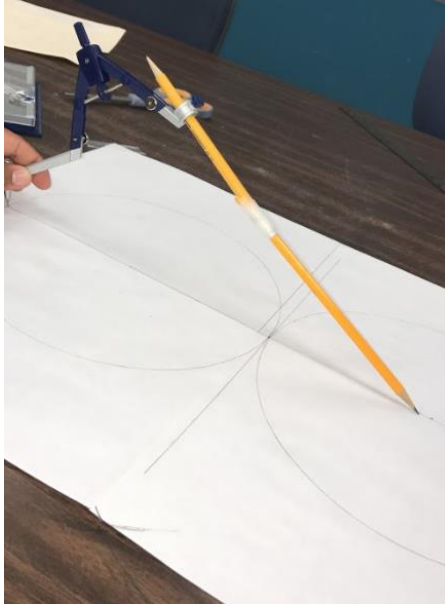
Figure 21: 2-D plan layout of oval-shaped surface

After the layout was drawn to scale on the poster, a 36"x36" aluminum sheet was used to construct the scour model. The thickness of the sheet was 0.02 inches and the surface texture was mill finish. This texture is very smooth as it has been machined with polishing but can cause oxidation if left outside or underwater for a long period of time. The sheet metal is shown in Figure 22 with the layout of the surface. In Figure 22, the centered oval represents the geometrical shape of the bottom surface of the scour hole that is subjected to be around the circular pile. As seen in figure 22, the height of the four triangular shapes on all sides of the oval is equal to the slope of the scour.

Figure 22: 0.019" Aluminum Sheet Metal with proposed layout plan

The tools used to construct the scour are shown in Figure 23. The next step was to cut through the black-marked lines in the metal sheet using one of the steel cutters shown in Figure 23.

Figure 23: Tool supplies for constructing the scour model

After cutting through the marked lines, the metal sheet was used to form an elliptical structure. The elliptical cone was tied from all 4 sides using screws and #6-32 machine screw nuts. The sheet metal was drilled by a shaft to form holes before placing the screws. The complete model is shown in Figure 24.

Figure 24: The completed 3-D scour model shown upside down.

The bottom surface of the concave-shaped scour model was inserted through the pile and into the tank. The scour model is then set on top of the river pebbles' reference line shown in Figure 25.

Figure 25: Concave-shaped Scour model around the pile

In Figure 20, the soil profile in the experimental schematic shows a fine, cohesionless sand layer with a depth of 12 inches. The total volume, V_t, of the sand layer is 22,531 in^3. Each sand bag contained a volume equaling to 1,024in^3, leading to a total of 22 paver sand bags that were needed for the pour. All of the bags were poured on top of the river pebbles and is illustrated in Figure 26. Figure 26 shows the experimental setup of the tank with a stabilized circular pile and simulated scour hole within the soil stratum. The four cardinal directions (North, East, South, West) were labeled in the tank

Figure 26: Simulated Local Scour under dry streambed condition

3.4.2.2 CASE STUDY II

Case study II presents a 3-D concave-shaped scour model setup with a known depth of 6.5 inches. The dimensions were determined by referring to the range of the angle of repose ($30°$- $44°$) for cohesionless soil. The first step of the procedure was to calculate longitudinal length of the scour with an angle of repose of $30°$. The diameter of the bottom

surface was assumed to be 8 inches. Figure 27 illustrates a sketch of the longitudinal length that was drawn in AutoCAD.
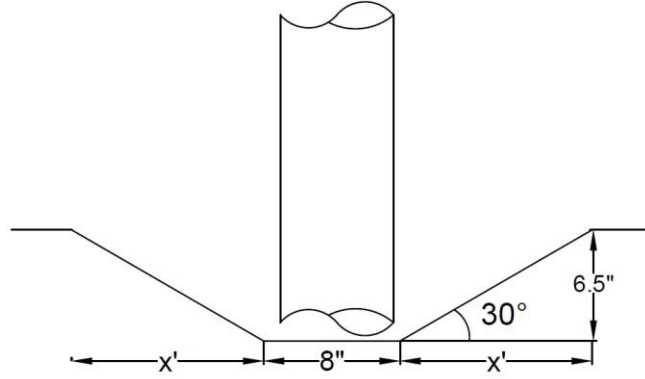
Figure 27: Longitudinal sketch of the scour hole

The sketch in figure 27 provides a visualization of the known angle of repose and scour depth. These parameters were incorporated into an equation to solve for X'. The symbol X' represents the unknown segment starting from the edge of the base to the edge of the scour hole. The equation is as follows:

$$tan\theta = \frac{Opposite}{Adjacent} \rightarrow tan30° = \frac{6.5\ inches}{X'}$$

$$X' = \frac{6.5\ inches}{tan30°} = 11.26\ inches$$

The next step was to calculate the total length, l_s, of the scour surface by computing the equation as seen below:

$$l_s = 2X' + 8 = 2(11.258) + 8 = 30.5\ inches$$

The relative scour length, L_s, is calculated below:

$$L_s = \frac{l_s}{b} = \frac{30.5}{6.625} = 4.61$$

43

The next step of the procedure was to solve for the transverse width of the scour hole. The known angle of repose is $44°$ which is to be used to solve for the unknown segments, X'. The diameter of the bottom surface was assumed to be 7 inches as seen in Figure 28.
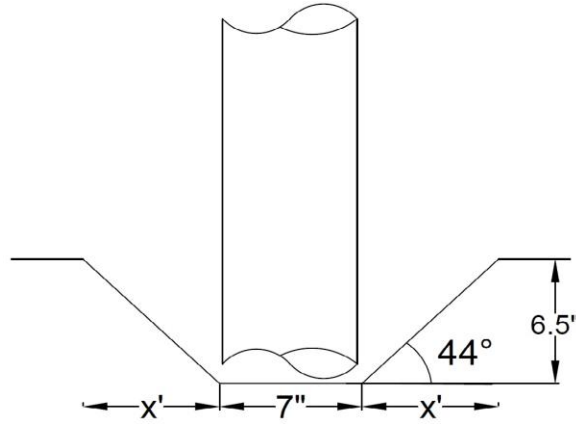
Figure 28: Transversal sketch of the scour hole

The calculations are as follows:

$$tan\theta = \frac{Opposite}{Adjacent} \rightarrow tan44° = \frac{6.5\ inches}{X'}$$

$$X' = \frac{6.5\ inches}{tan44°} = 6.7\ inches$$

The next step was to calculate the total length, l_s, of the scour surface by computing the equation as seen below:

$$l_s = 2X' + 8 = 2(6.7) + 7 = 20.4\ inches$$

The relative scour length, L_s, is calculated below:

$$L_s = \frac{l_s}{b} = \frac{20.4}{6.625} = 3.08$$

The plan view of the scour model is seen in Figure 29.
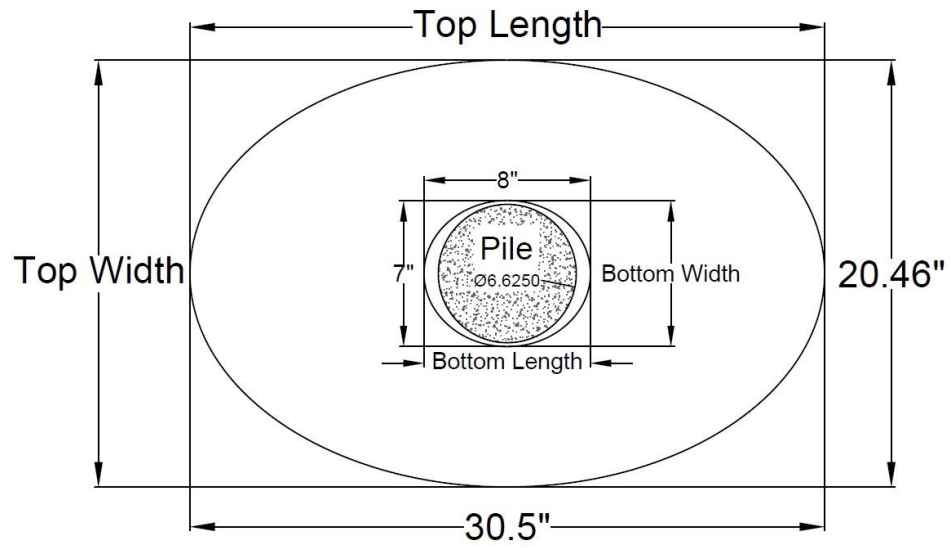
Figure 29: Plan view of the scour model

The longitudinal and transverse cross-sectional views of the scour hole are shown in Figure 30.
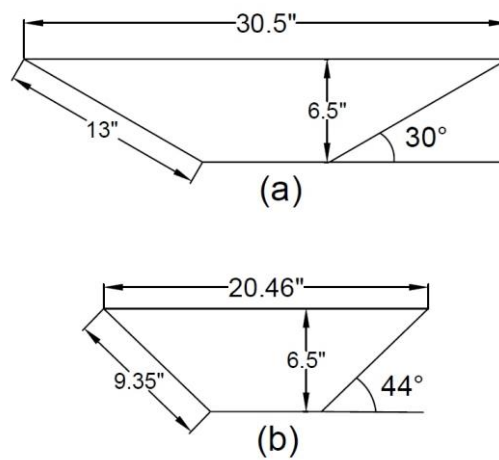
Figure 30: (a) Longitudinal cross section; (b) Transverse cross section

The experimental schematic presented in Figure 31 has a distinctive soil profile than the profile from case I; the cohesionless soil is at a depth of 6.5 inches and is in flush with the scour surface, and the height of the water column is 14 inches.
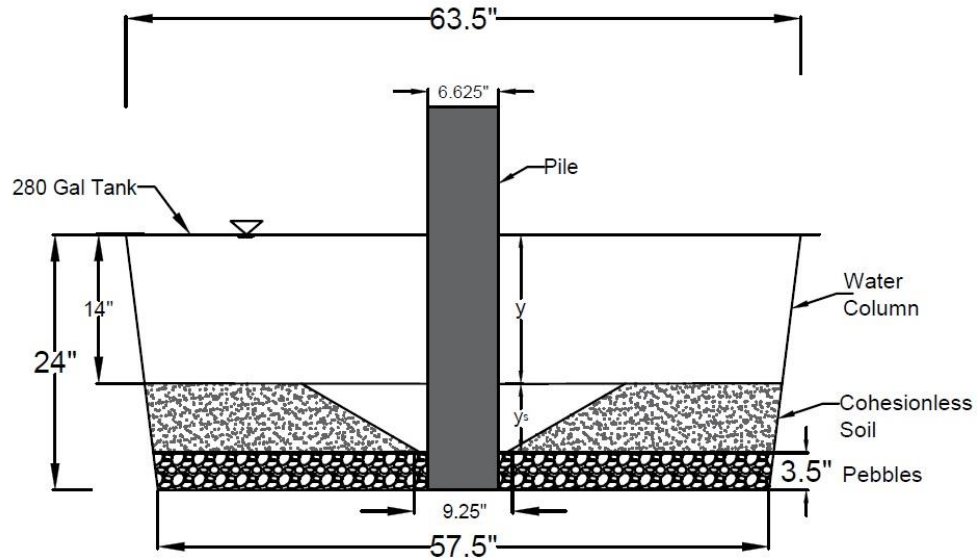
Figure 31: Experimental schematic of simulated bridge pier local scour

A 2-D plan of the scour hole was drawn to scale on a poster. The plan contains the layout of the oval-shaped surface along with the dimensions. A different technique was used to draw the oval in the plan, as opposed to the first case. The first step was to draw an oval with the calculated dimensions via compass. The layout is illustrated in Figure 32.

46
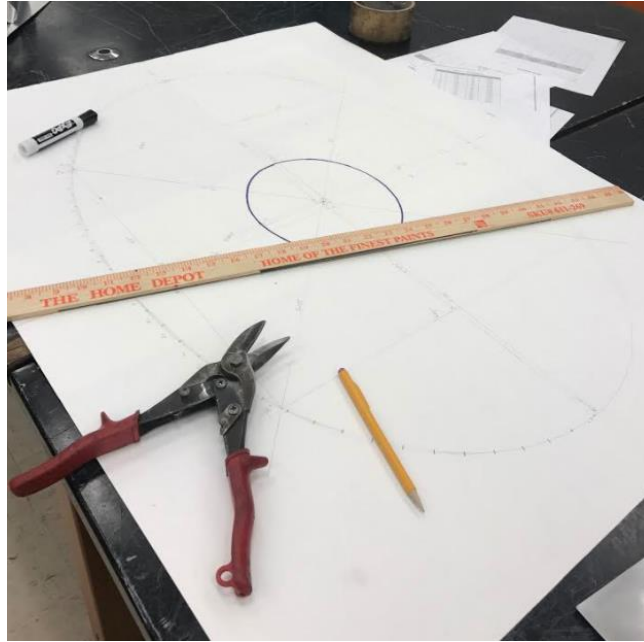
Figure 32: 2-D plan layout of oval-shaped surface

The aluminum sheet metal and tool supplies are shown in Figure 33. The same procedure was followed from the case I to construct the scour model.

Figure 33: Alum. Sheet metal and tool supplies

After constructing the scour model, it was placed in the tank around the pile as seen in Figure 34. The purpose of the plastic sheet shown in the figure is to prevent water from being suspended, and to maintain clear water.

Figure 34: Simulated Local Scour with plastic sheet

3.4.3 HYDROLITE-TM INTRUMENTATION

The purpose of this study is to utilize the HydroLite-TM instrument to measure the scour depth of known dimensions. This is a sonar-based method that allows the transducer at the bottom of the rod to transmit sound pulses to the riverbed and return back up to store the elevation readings in the data collector. The advantage of using this instrument is that it quickly measures and logs depths more accurately than standard systems. This procedure has been done for two cases. In the first case, the soil column was 8.5 inches deep and in the second case, the soil column was reduced to 6.5 inches.

3.4.3.1 EXPERIMENTAL SETUP

The HydroLite-TM equipment kit includes the following:

- SonarMite BT MILSpec Echosounder kit

- Transducer, 200kHz, 9deg

- Internal rechargeable 12V battery

- HydroLite boat mount/pole kit

- Ping rate: 6 Hz

- Depth accuracy: 1 cm/0.1 percent of depth

- Output formats: NMEA, ASCII, Quality

- Operating range: 0.3 m – 75 m

- Rugged shipping case

- Quick Start Guide/User Manual

The HydroLite-TM sonar works properly when it is screwed to a mounting bracket. The mounting bracket allows the sonar to be stable and prevents it from shaking or moving. The mounting bracket allows the sonar to transmit and receive sound pulses without any interruption, and records accurate data. In order for the sonar to collect accurate readings from the water surface to the bottom of the tank, it must be placed in a fixed position. Consequently, a set of two 2 x 4 plywood was mounted on top of two barrels that are positioned on each end. Figure 35 depicts the set of plywood that is resting on the barrels above the tank. The purpose of the plywood is to tie the sonar rod onto the mounting bracket that is screwed to the plywood.

Figure 35: Configuration of the sonar positioning

After placing the plywood on the barrels, the mounting bracket was attached and tightly screwed to the plywood as shown in Figure 36.

Figure 36: Sonar mounting bracket screwed to the plywood

The HydroLite-TM sonar rod is divided into three sections and was assembled in the laboratory. The total length of the rod with the 3 sections screwed to each other was 6 feet. After screwing the sections together, it was placed vertically into the mounting bracket as shown in Figure 37.

Figure 37: Attachment of sonar rod to mounting bracket.

The transducer and the Echosounder were attached to their proper locations in the rod. The transducer was attached to the bracket at the bottom of the rod. The transducer's cable was connected to the SonarMite Echosounder's input. Figure 38 illustrates the attachment of the GPS unit and transducer to the sonar rod. The GPS unit was screwed to the top of the rod, which was used to track nearby satellites for world imagery. As seen in Figure 38, the serial cable of the Echosounder was connected to the transducer's input. This is to transfer sound pulse readings from the transducer to the Echosounder. The Echosounder will then transmit the data to the controller via Bluetooth.
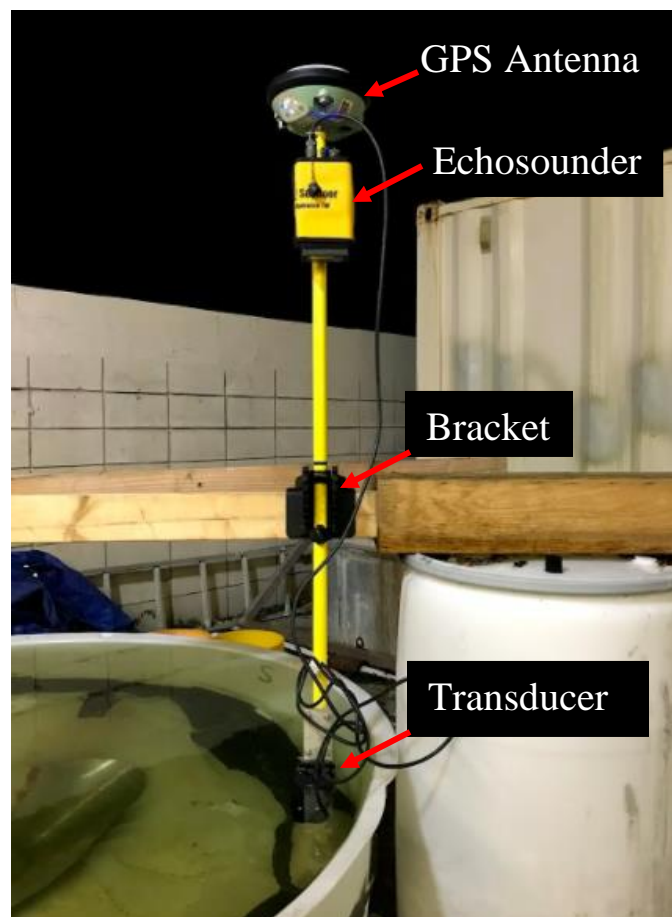
Figure 38: GPS Antenna and Echosounder Attached to Sonar Rod

Figure 39 illustrates the attachment of the controller to the sonar rod. The controller is a wireless device that receives data from the Echosounder and world imagery information from the GPS unit.

Figure 39: Attachment of controller unit to sonar rod

After connecting all instruments to the sonar rod, the sonar was ready to perform a hydrographic survey across the tank in straight lines. The transducer at the bottom of the rod is maintained in a stationary position on the surface of the water for collecting the elevation points as the rod is positioned along the plywood. The plywood on top of the barrels allows the attached sonar rod to slide in straight lines from the outermost curvature of the tank to the cylindrical pier exterior surface. For every inch travel along the plywood,

the sound pulses from the transducer transmit a signal to the Echosounder. The transducer

then sends a signal via Bluetooth to the data collector unit, and that is how the elevation of

data points is logged for each 1-inch increment.

Figure 40: The sliding of the rod from the end of tank to
the center of the scour

3.4.4 GREEN LASER INSTRUMENTATION

This study deals with a method using laser-based optical approach instrumentation

to measure the scour depth around a model circular pier. The laser-based optical approach

utilizes the Terrestrial Laser Scanner (TLS) Leica ScanStation II to transmit a green laser.

This instrument is a pulsed, dual-axis, compensated, very-high speed laser scanner, with

survey-grade accuracy, range, and field-of-view. The green laser scanner will measure a 3-

D concave-shaped scour hole with known dimensions.

3.4.4.1 APPARATUS

The technical equipment used in the experiment was the Leica ScanStation II laser scanner, a survey level, a survey tripod, white-dotted targets, serial cables, and a laptop containing Cyclone Software. Figure 41 illustrates all equipment that was used in the experimental process. The Leica scanner is about 41 pounds and is kept in a rolling weatherproof hard case. The red bags in the figure contain the targets. The targets were placed in 6 different locations around the laser scanner to perform the target-based registration, which is further discussed in the chapter.

The standard accessories included are:

- Scanner transport case

- Tribrach (Leica Professional Series)

- Survey Tripod

- Ethernet cable for connection of scanner to PC

- Two Power Supply Cases. Each includes:

  i) Power Supply

  ii) Cable for battery connection to scanner

- User manual

- Cleaning kit

- Cyclone-SCAN software

Figure 41: Green Laser Equipment

3.4.4.2 STATIONS 1,2, AND 3

Leica ScanStation II transmits a green laser with 532nm wavelength and 4 mm range accuracy to scan the entire local scour region. Firstly, the TLS was assembled on one side of the test tank so as to have a maximum coverage of the scour hole. Due to the perspective of the TLS, it is not possible to scan the complete scour hole from only one station. Therefore, a second and third station were needed to cover the remaining portions of the scour hole. By using three stations, the scour hole was scanned in the dry condition without water to derive the base data.

The assembly of the scanner was done at the experimental location of the scour setup. For cases I and II, the survey tripod was aligned at 6 feet C-C from the center of the model bridge pier. The survey level was placed on top of the tripod. Cases I and II had a series of 3 stations for dry condition and clear water condition. The following procedure of

the green laser setup pertains to each case in all the three stations. Figure 42 illustrates a general schematic of the green laser setup for any station.
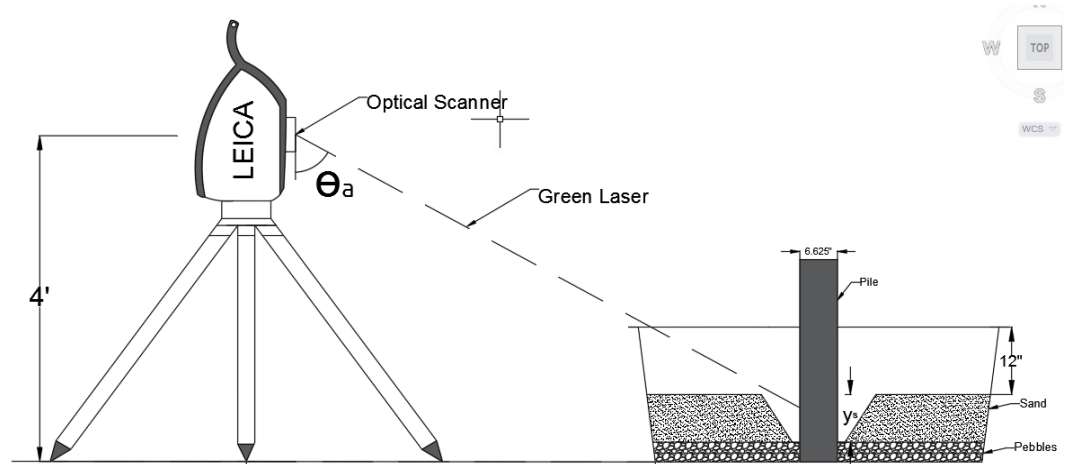
Figure 42: Green Laser configuration per each station

The first step was to assemble and level the tripod on the ground and the optical-based laser is now ready to scan the entire soil stratum and the scour hole.

Figure 43: Assembly of the Tripod 6 feet from the
Bridge Pier Model.

As shown in Figure 43, the tripod is placed on the three-sided members at the base and is stabilized by rubber bands. The slab on grade on which the tripod is resting on has a gentle slope. Therefore, the tripod must be leveled in order for the green laser to function properly. As seen in Figure 44, the bubble on the survey level appears to be centered, which means that the tripod is leveled and is ready for the placement of the green laser. The bubble was brought to the center by rotating the rollers on each side of the survey level clockwise and counterclockwise, and by adjusting the height of the pods.

Figure 44: Depiction of the survey level and the centered
bubble at the top right

After leveling the tripod, the next step was to carry and mount the Leica green laser

scanner onto the survey level. The scanner is shown in Figure 45. The Leica ScanStation 2

was carried out of the box and mounted on top of the survey level as shown in Figure 46.

Figure 45: Leica ScanStation 2 Laser Scanner

Figure 46: Attachment of Laser Scanner to Survey Level

The base of the scanner is resting on the survey level and shown in Figure 46. At the bottom of the scanner, there are 2 metallic vertical hooks that penetrate through the holes at the survey level (the holes are shown in Figure 44) to stabilize the scanner. Since the survey base is leveled, the scanner becomes leveled and is in a fixed position. After the placement of the scanner, the next step was to allow the scanner to make a 360-degree rotation about the y-axis by pulling the black handle shown in Figure 47. This handle is pulled and then turned counterclockwise to allow free movement of the scanner as it rotates during a scanning session. The black cable shown in Figure 47 is the power cable connecting the scanner to the power supply. The white cable is the Ethernet cable connecting the scanner to the laptop to transfer the scanned data to Cyclone software. The green light means that the laser scanner is ready to perform a scanning session and the red light means that the scanner is in the process of scanning.

Figure 47: Illustration of Power and Ethernet inputs.

The next step was to assure the height of the laser scanner was at 4 feet O.C. from the slab on grade. The height of the scanner was measured at 4 feet O.C. and is illustrated in Figure 48.

Figure 48: Illustration showing a 4-Foot height of laser scanner from the Slab.

3.4.4.3 DRY CONDITION

The experimental procedure for dry condition pertains to cases I and II in this process. The purpose of this condition is to perform a vertical and horizontal 3D laser scan of the scour hole to collect point cloud data. A 3D laser scan was conducted at 3 different stations around the tank.

Figure 49: Station I Location

Figure 49 illustrates the location of station 1 to be north of the tank at a 6-foot distance from the model bridge pier. As shown in Figure 49, the laser scanner is connected to the power supply via black cable and connected to the laptop via ethernet cable. The laptop displayed the Cyclone software, which provided 3D scan within the station region and calculated the amount of time per scan session.

The next step was to add 3 circular targets with a white dot in the center around the tank, and is illustrated in Figure 50. Each target was placed in a different location; one in the northeast, one in the southwest, and one in the northwest of the tank. In each station, the emission of the green laser will scan those targets along with the scour hole to perform the target-based registration in Cyclone to combine the scans from the 3 stations into one

whole scan. This process will remove unwanted areas, such as shadows and any incomplete areas with insufficient point clouds.

Figure 50: White-Dotted Target

Figure 51: Location of targets in Station I: Northern Region

Two of the targets are shown in Figure 51: - one on the far right standing on a white

bucket, and another on the far left standing on a table. The white-dotted targets are facing

the laser scanner so that they are clear and visible in the 3D scan. The location of the

scanner corresponds to station 1. After the scan within the region in station 1, the 3D scan

data was transmitted to Cyclone Software.

The scanner is now shifted to the second station and shown in Figure 52. The second

station was located at the southwest side of the tank. The scanner collected point clouds in

the vertical and horizontal directions and scour model of that specific region was scanned

and transferred into Cyclone software. Now, Cyclone has collected 3D scanning data of

two distinct regions. The third station was needed to complete the scanning over the entire

scour hole.

Figure 52: Location of Station II: Southern Region

The scanner was then shifted to the third station located at the northwest side of the tank.

Figure 53: Location of Station III: Northwest Region

The third station is shown in Figure 53. The scanner emitted a laser that scanned the final region, which was not previously scanned by the first and second stations. The scans of the 3 stations were stored in Cyclone Software and were all combined into one whole scan, representing the 3D image of the entire scour hole. The combined 3D image will allow the user to determine the geometry of the scour hole under dry condition.

3.4.4.4 CLEAR WATER CONDITION

The tank is now filled with water to a depth of 12 inches for Case I study. After completing the 3D scan for dry condition, the same procedure adopted for the dry condition was used for the clear water condition. Cases I and II had water columns of 12 and 14 inches respectively. In this procedure, 3 stations were used around the tank for both cases. During the scanning sessions in each station, the laser penetrated through the water column and scanned the scour hole while submerged. The angle at which the laser is emitted from the scanner to the water surface has changed due to water refraction. The water refraction caused a distortion in the imaging process as data was being transferred to Cyclone Software. A refraction correction was applied and the results are shown in the *Results and Discussion Chapter.*

Tracing back to Figure 34, a plastic membrane was spread over the top surface of the entire soil stratum as well as the interface between the interior wall surface and the soil stratum. This procedure was used essentially to prevent water seepage and formation of fine soil particle suspension in the water. This procedure enabled maintaining clear water conditions and measurement of scour hole profile using green laser. Firstly, water was hosed into the tank for approximately 15 minutes until the water was flushed to the test tank's rim at the surface. Figure 54 shows the test tank in clear water condition with a water depth of 12 inches.
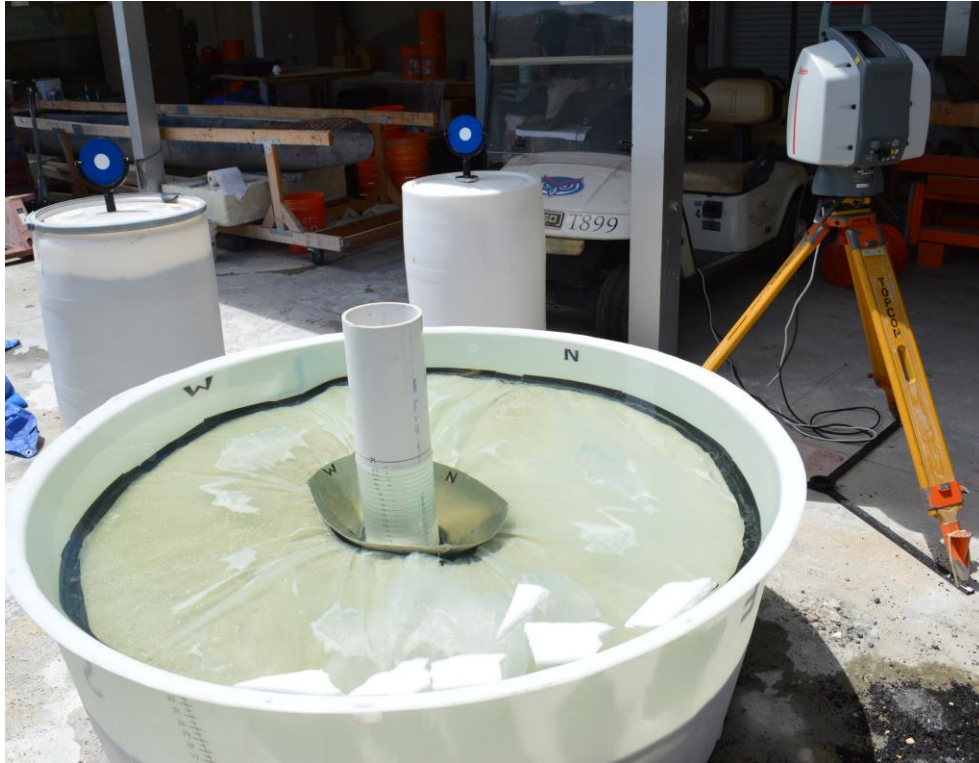
Figure 54: Simulated Local Scour setup with water depth of 12 in.

The water-filled test tank was ready for a scanning session and Figure 55 shows the location of station 1. The optical-based scanner at station 1 was located north from the test tank to scan the northern region of the scour hole. The 3 white-dotted targets were placed around the tank for the laser scanner to capture their image. Figure 55 shows the orange cords, which were attached from the holes at the rim to the top of the model bridge pier to maintain its stability during the scanning session. The soil stratum was 10 inches deep, with a scour hole of maximum depth of 6.5 inches (Case II), and with a 14-inch depth water column. After the scanning session was completed in station 1, the laser scanner was moved to the second station in the eastern region and illustrated in Figure 56.

Figure 55: Location of Station I: Northern Region

Figure 56: Location of Station II: Southern Region

The laser scanner emitted a green laser throughout the eastern region and transmitted the data to Cyclone Software. After the scanning session was completed, the final step was to move the scanner to the third station. The third station was located on the northwestern region and is shown in Figure 57. The survey level was readjusted to accommodate for the changed elevation of the slab at the 3rd station point.

Figure 57: Location of Station III: Western Region.

3.5 SOIL/SEDIMENT PROPERTIES

The soil profile within the local-scour region consists of cohesionless sediments and gravel. The angle of repose of cohesionless soil in the profile falls in the range of $30° − 44°$, which gives the sense that the slope of the local scour is not very steep.

3.5.1 SIEVE AND PARTICLE ANALYSIS

The grain size characteristics of the soil and pebbles around the foundation pile were evaluated by a sieve analysis. A nest of sieves was prepared by stacking test sieves

one above the other with the largest opening at the top followed by sieves of successively

smaller openings and a catch pan at the bottom. The nests were placed into the shaker for

10 minutes and the aggregates were evenly distributed as shown in Figure 58.

Figure 58: Evenly distributed particles after the shake

Opening mesh sizes of commonly used sieves are shown in Table 1.

Table 1: Sieve Analysis Table

Sieve No.	Sieve Opening (mm)	Mass of retained soil (g)	Percent of Mass Retained	Cumulative Percentage %	Percent Finer
0.38	9.5	294.85	18.84	18.84	81.16
4	4.75	217.87	13.92	32.77	67.23
8	2.36	292.03	18.66	51.43	48.57
16	1.18	323.82	20.70	72.13	27.87
30	0.6	394.38	25.21	97.34	2.66
50	0.3	33.33	2.13	99.47	0.53
100	0.15	6.84	0.44	99.90	0.10
Pan		1.49	0.10	100.00	0.00

After computing the percent finer for each sieve, the results were used to form a logarithmic graph of the percent passing versus the sieve size. The graph is shown below.
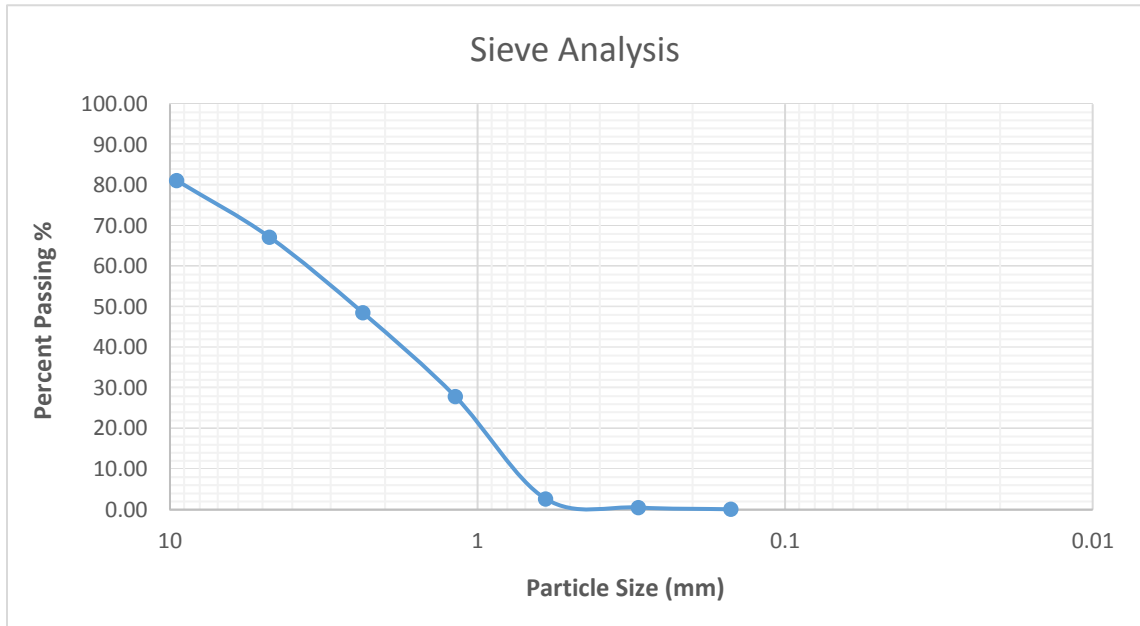
Figure 59: Particle-Size Distribution Curve

From the sieve analysis semi-log graph shown above, the mean particle size D_{50} was equal to 2.55 m. The effective diameter size D_{10} in the particle-size distribution curve corresponding to 10% finer is 0.77 mm. From the distribution curve, the diameter size D_{60} and D_{30} were found to be 3.75 mm and 1.32 mm respectively. The soil parameter known as the relation gives the uniformity coefficient:

$$C_u = \frac{D_{60}}{D_{10}} = \frac{3.75\ mm}{0.77\ mm} = 4.87$$

The uniformity coefficient was calculated using the equation shown above and was equal to 4.87. The coefficient of gradation is expressed as:

$$C_c = \frac{D_{30^2}}{D_{10} * D_{60}} = 0$$

71

CHAPTER 4: EXPERIMENTAL STUDY: RESULTS ANALYSIS AND

DISCUSSIONS

4.1 SCOUR MEASUREMENT USING GREEN LASER

The 3D-scan image processing and computations were completed using a software package called Leica Cyclone 9.1. Cyclone is a 3D point cloud processing software that lets users take advantage of traverse, back-sight, and resection capabilities of the Leica ScanStation C10 laser scanner. The inherent completeness of 3D point clouds represents one of the major advantages over other sources of geometric information. Cyclone's unique Object Database Client/Server software architecture provides the highest performance environment for laser scanning projects. Cyclone software makes it easy for users to manage data efficiently in databases. Users can work concurrently on databases, thereby reducing the need to copy and/or transmit large point cloud project files.

4.1.1 CASE STUDY I

For case study I, two stations were set up around the tank: the first station being situated at the northern region of the tank and the second station at the southern region.

4.1.1.2 DRY CONDITION

In order to combine the point cloud from the two stations, six targets were established around the scour setup. These targets are used to tie two point-clouds by target-to-target registration process with Leica Cyclone software. The registered point cloud of the simulated scour hole is shown in Figure 60. It could be noticed that under

dry condition (no water), 1.1 inches below the simulated scour hole could be captured, as shown in Figure 61. In addition, the width and length of baseline condition is within 1% of design dimensions. To demonstrate the underwater experiment, the tank was filled with water to its rim level. The setup of the water tank with simulated scour hole is shown in Figure 7. In order to determine the height of the water level, Styrofoam pieces were floated at the water level (Smith, et. al, 2012).
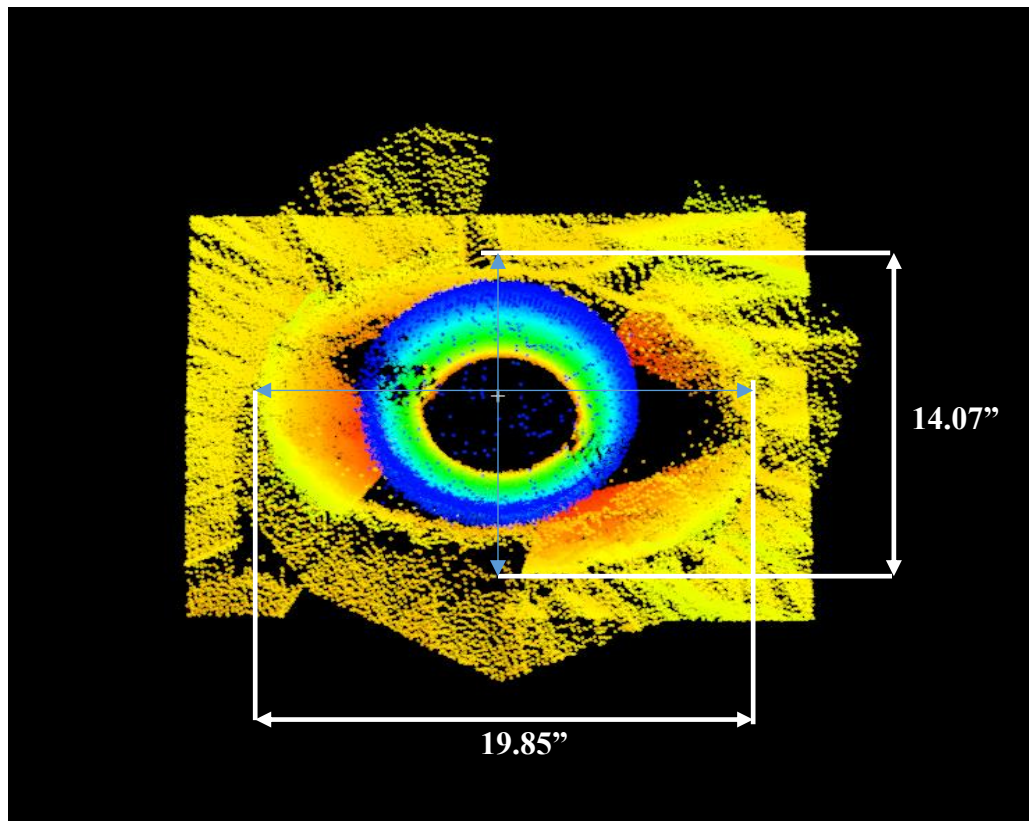
Figure 60: Plan view of The Simulated Scour Hole Without Water.
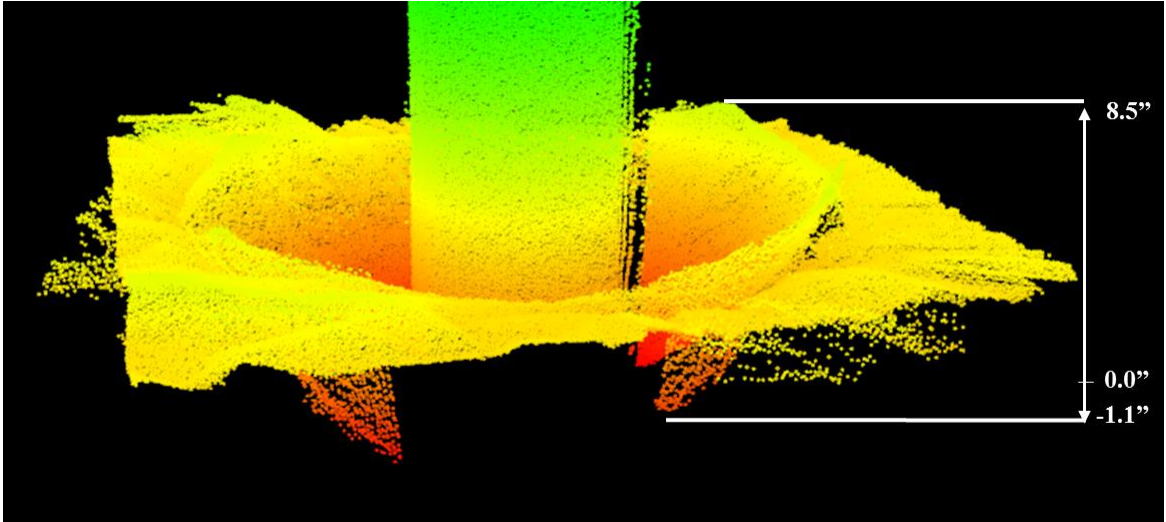
Figure 61: Front view of scour hole before filling with water.

4.1.1.3 WATER REFRACTION CORRECTION

Then laser scanning was performed at the first station and repeated on the second station with both scans covering full view of the scour hole. Note that these stations do not have to be identical to the stations used for without water setup as targets were kept fixed all the time. However, as shown in Figure 62, the laser pulse will get refracted after hitting the water level. Figure 62 illustrates the result of refracted point clouds from two stations. By using the mathematical model shown in Figure 14, the refraction correction was applied independently to the point cloud in both stations. The refraction correction was applied separately as the amount of correction is dependent on the angle of inclination of the incident laser pulse which will be preserved only when the origin (0, 0, 0) of the point cloud is at the corresponding laser scanner stations of the point cloud.
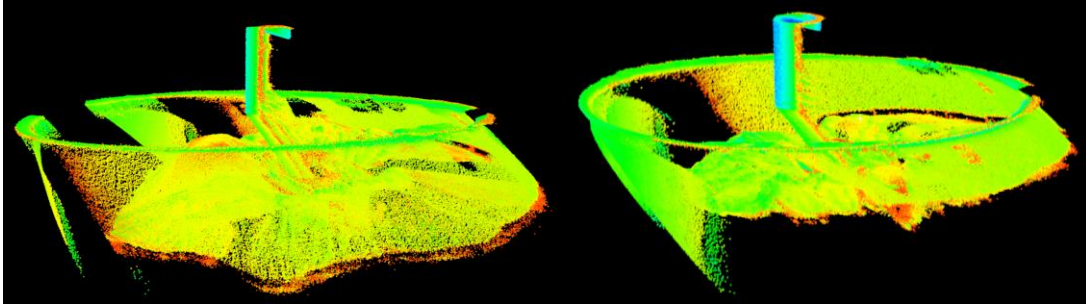
Figure 62: Station 1 and Station 2 Tank (side by side) before refraction correction

In order to perform the water refraction correction, the point clouds within the refracted area were fenced out of the modelspace in Cyclone and copied to a new modelspace. The refracted point clouds in the new modelspace were exported from Cyclone and were saved as a text file. The text file consisted of 3 columns (comma-separated) of point clouds containing the *X, Y, Z* data. This uncorrected text file was imported into MATLAB software to run a series of codes that will correct the data. The code in MATLAB will change the original, distorted image to the correct image, which will provide a more accurate image of the scour hole while submerged.

After loading the uncorrected text file into MATLAB and running the code, the corrected file was made and saved in a different name. This procedure was performed for both stations. Finally, the corrected point clouds were imported to Cyclone and were loaded onto the same region of the original point clouds. The corrected point clouds were aligned properly in the original region and the images are shown in Figures 63 through 64.
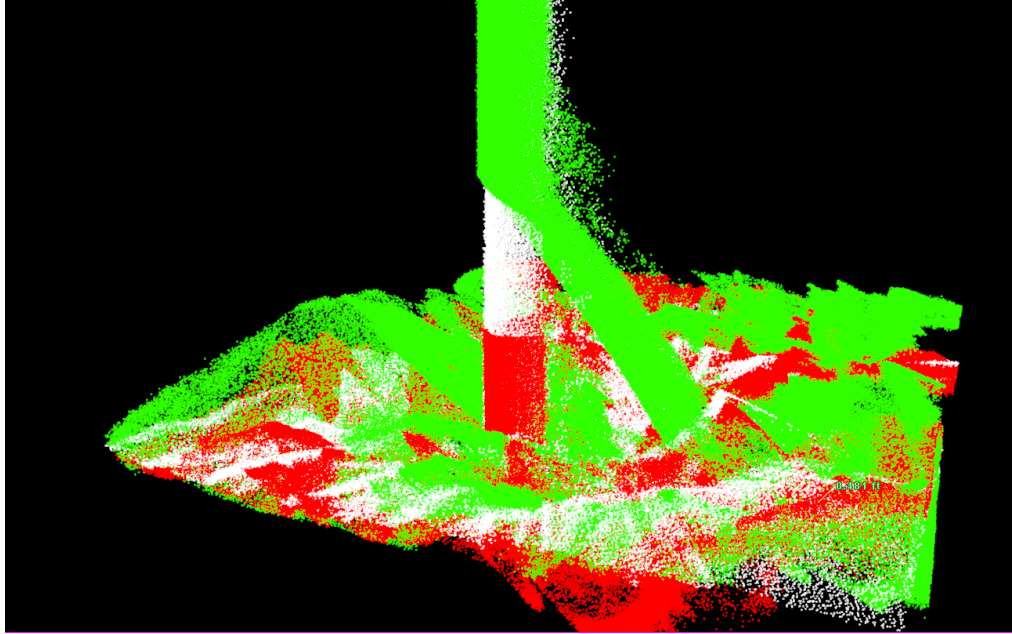
Figure 63: Alignment of Corrected Point Clouds Shown in Red and White
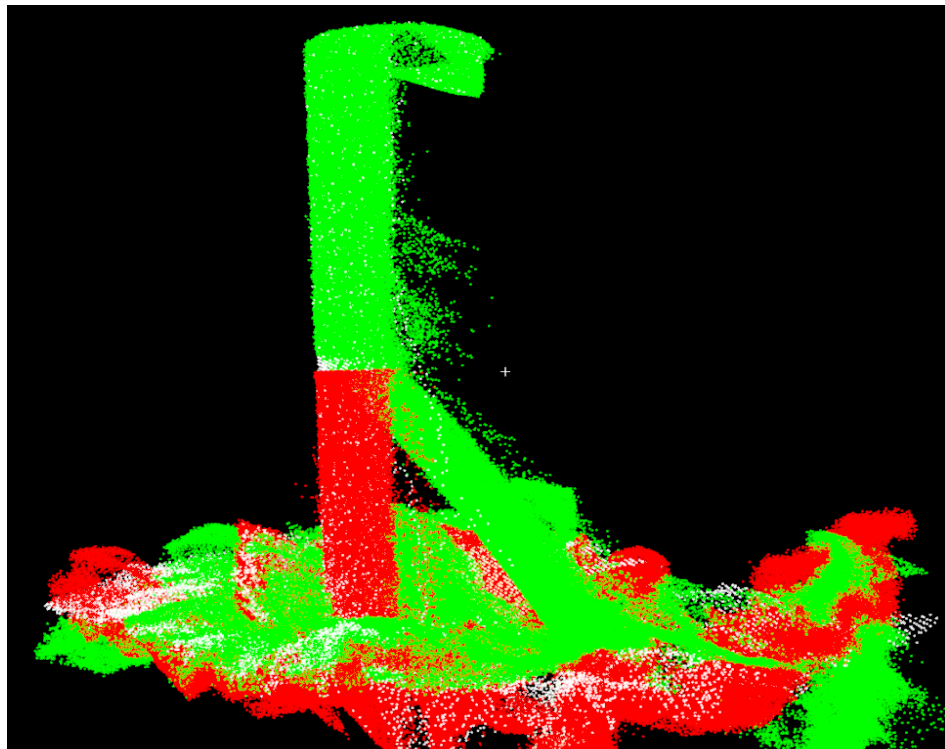
Figure 64: Alignment of Corrected Point Clouds Shown in Red and White

After the importation of the corrected data into both of the 3D scan stations, the corrected point clouds were properly aligned in the fenced-out region, where the original refracted point clouds previously existed. The Cloud-To-Cloud registration process was performed to combine the two corrected scans into one whole scan. The results of the corrected point clouds for both stations are shown in Figures 65 through 66.
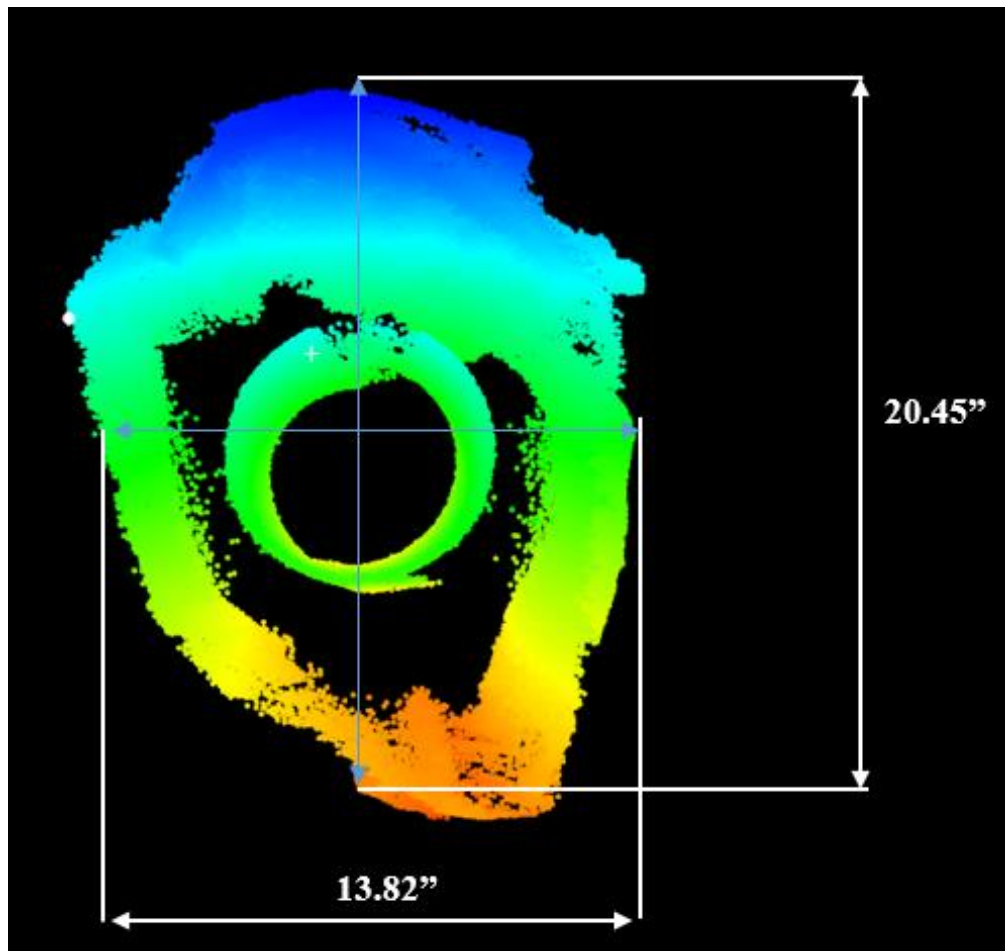
Figure 65: Plan View: Showing Dimensions of the simulated Scour after Refraction Correction
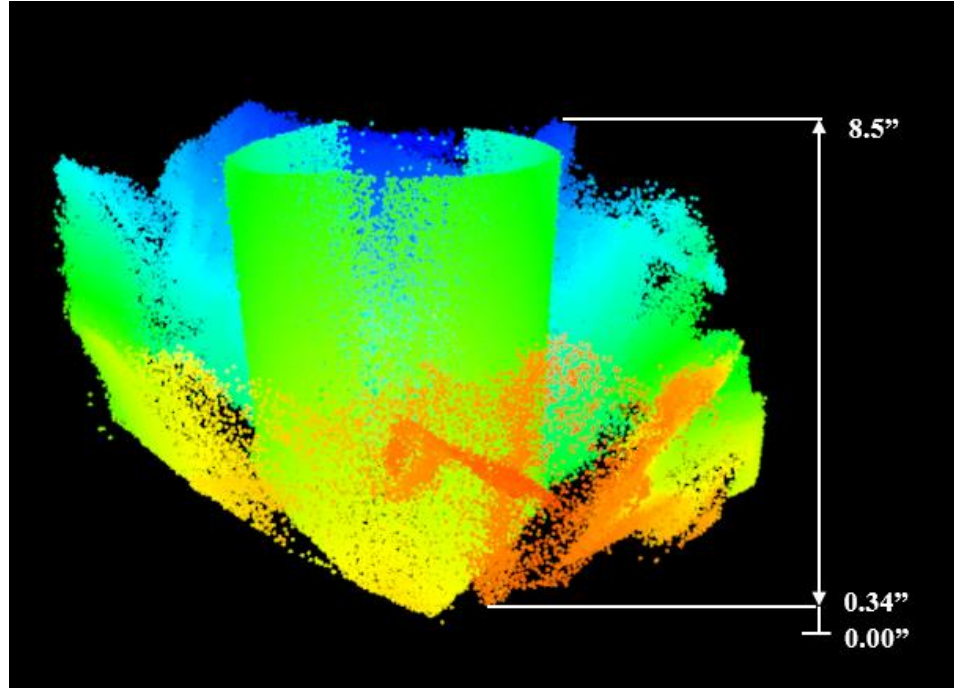
Figure 66: Front View: Simulated Scour after Refraction Correction.

The corrected length and width of the simulated scour hole is within 1% of the design dimensions after the refraction correction. However, unlike the baseline condition where 1.1 inches below the scour could be seen, the submerged scour could only be captured from 0.34 inch from the bottom. It could be inferred from the illustration that the noise is high, especially near the water surface and underwater. Moreover, the data collection in bright daylight caused a higher scattering of the green wavelength laser to increase the noise. Despite the issue, the scour can be reconstructed using the demonstrated non-contact technique.

In order to evaluate the accuracy of the reconstructed scour model, it was compared with the point cloud that was created without water. The comparison was performed after manually removing the noise in the data sets. Cloud-to-Cloud distance function in CloudCompare (Khawairakpam, et. al, 2012) was used to determine the mean distance

between the point clouds. The mean distance error was computed as 27 mm. Despite having some absolute positioning error, the relative shape of the reconstructed scour model after refraction correction is identical to the original setup as shown in Figure 60, where the dimensions are consistent with design values. The factors that might have caused high distance errors are turbidity of the water, assumption of 1.33 for the refractive index which could be higher or lower, high existence of noise due to high reflectivity of the aluminum scour model.

4.1.2 CASE STUDY II

The results in case study II pertain to the simulated scour model with a known depth of 6.5 inches. The 3D-scan project files for each station were saved in the server in Cyclone Software shown in Figure 67.
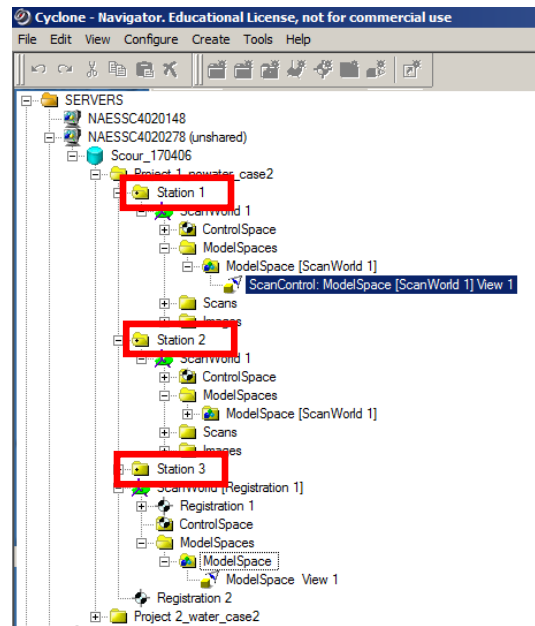
Figure 67: Cyclone Software Server

4.1.2.1 DRY CONDITION

The 3D-scan images of the scour hole for each station are shown in Figures 68 through 70.

79
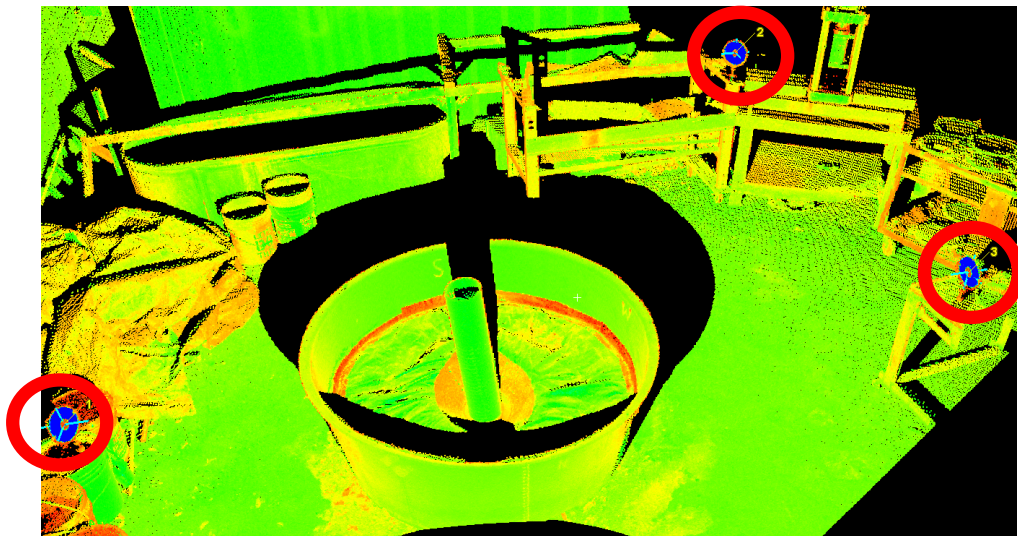
Figure 68: 3D-Scan Image from Station I Looking South.

Figure 69: 3D-Scan Image from Station II Looking Northwest.
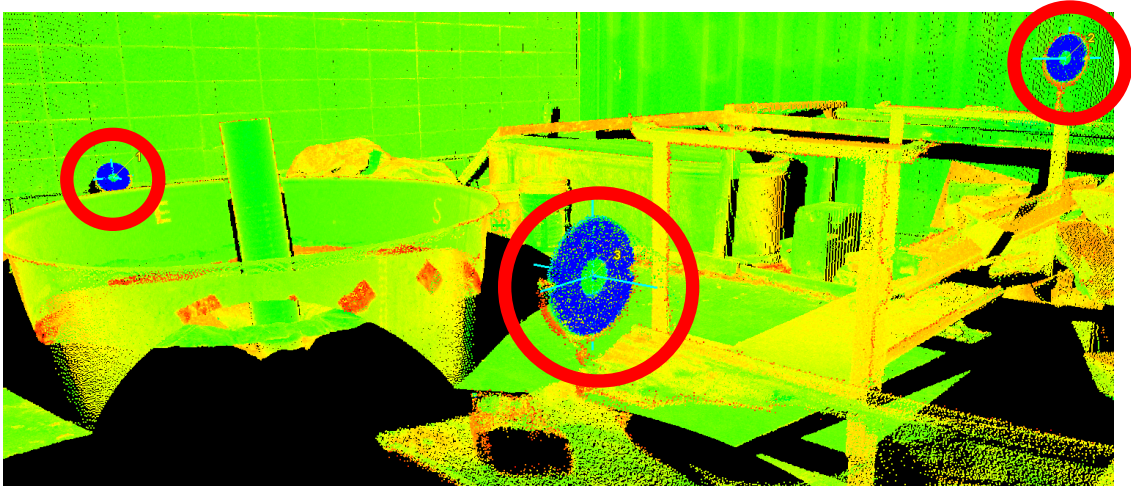
Figure 70: 3D-Scan Image from Station III Looking East.

The targets in Figures 68 through 70 are circled in red. The purpose of these targets was to perform the target-based registration to combine the 3 scans into one whole scan that contains the complete image from all angles. However, one of the targets in station II (Figure 69) was not captured during the scanning session. Therefore, this has led to an insufficiency in targets and would complicate the process of performing the target-based registration.

Consequently, the cloud-to-cloud registration was performed instead. This method accommodates for measuring overlapped distance. Instead of matching the targets in station I or II with station III, the point clouds would be matched between each station. The point clouds that were chosen in station I scan were matched with the point clouds chosen in either station II or III; three point-clouds of each station were selected. The cloud constraints were made between 2 stations (windows) at a time as shown in Figure 71. After opening the cloud constraints shown in Figure 71, 3 points were selected on each window in corresponding positions.
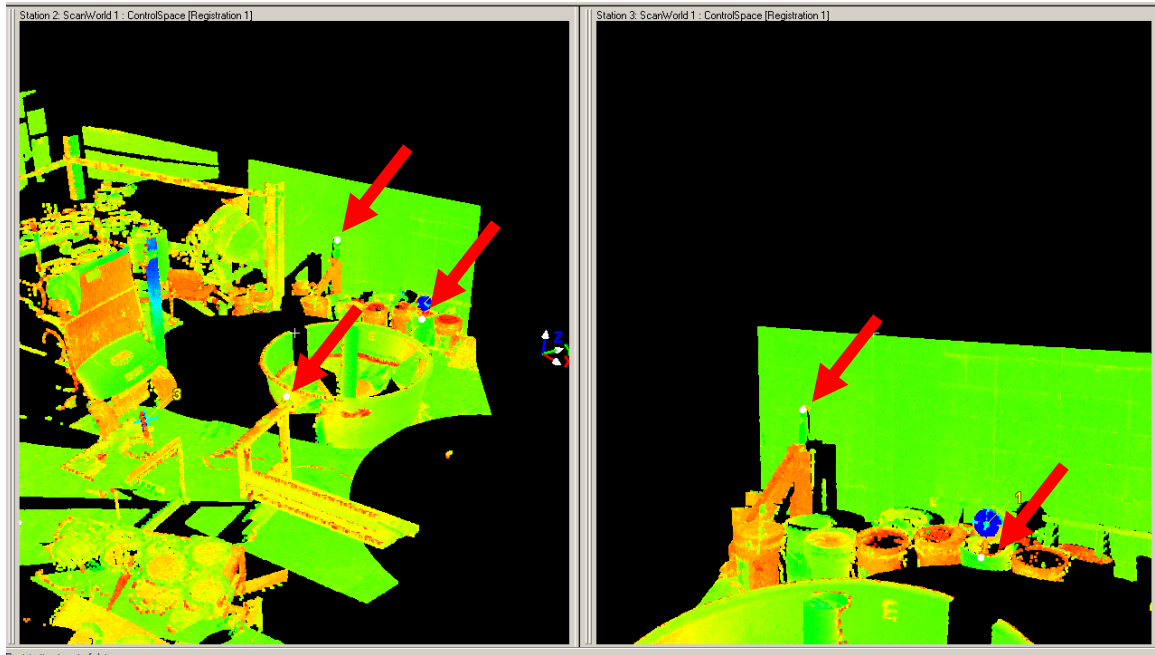
Figure 71: Cloud-To-Cloud Registration between Station II and III.

In Figure 71, the arrows point out the selected matching clouds from each window. After selecting the points on each cloud in corresponding positions, the cloud mesh was selected under the constraints tab to view the interim results. This allowed for a new modelspace to open and display the three point-clouds fitted together. After the completion of the registration, the unnecessary point clouds that surround the scour hole region were eliminated. The fence tool in Cyclone was used to remove the irrelevant clouds. The new image of the scour hole is shown in Figures 72 through 73.
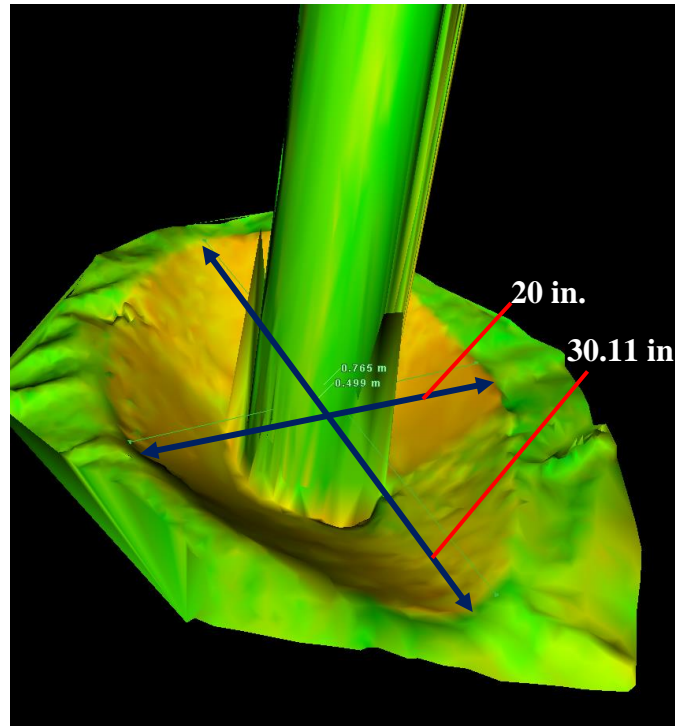
Figure 72: 3D Mesh Isometric View of 6.5-Inch Scour Hole
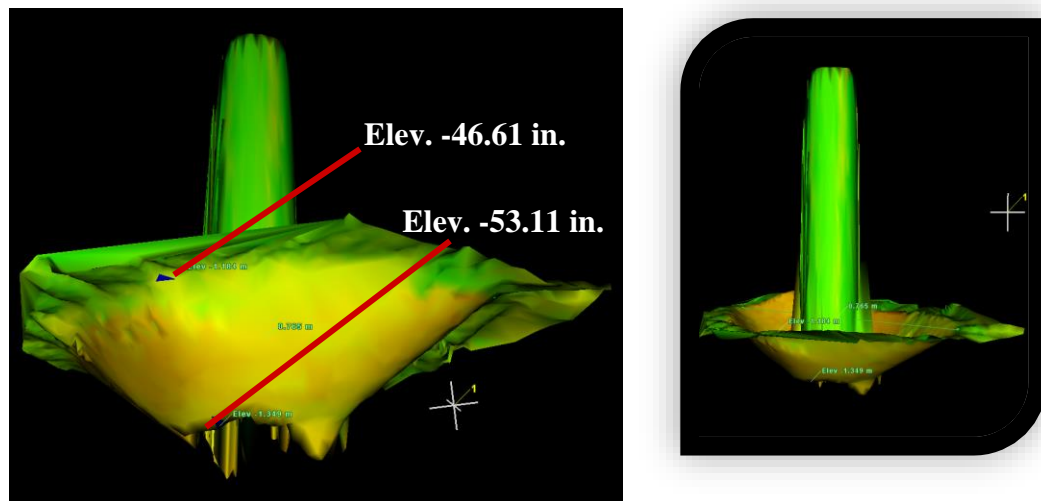
Figure 73: Elevation View of Scour Depth

In Figure 72, the 3D mesh represents an isometric view of the scour hole around the bridge pier model. It illustrates a longitudinal dimension of 30.11 inches and a transverse dimension of 20 inches, which are very close to the actual dimensions of the

aluminum scour model. In Figure 73, the elevation view of the scour hole is shown. Initially, the scour model had a known depth of 6.5 inches. The top of the scour hole shows an elevation of -46.61 inches from the laser scanner's reference point. The bottom of the scour hole shows an elevation of -53.11 inches from the laser scanner's reference point. The difference of the top and bottom elevations is 6.5 inches. This concludes that the measured depth has matched with the actual depth measurement of the real shape.

4.1.2.2 WATER REFRACTION CORRECTION

The laser beam was emanated from the origin (0,0,0) at an angle θ_a and traveled through the airborne medium and into the water surface. As the laser beam penetrated through the water surface, the angle was changed to θ_w in the water column. Water refraction has caused the path of the laser beam to be altered to an angle θ_w starting from the water surface to the riverbed. Therefore, the scanning sessions in stations I, II, and III have resulted in distorted images due to water refraction. The refracted images are shown in Figure 74.
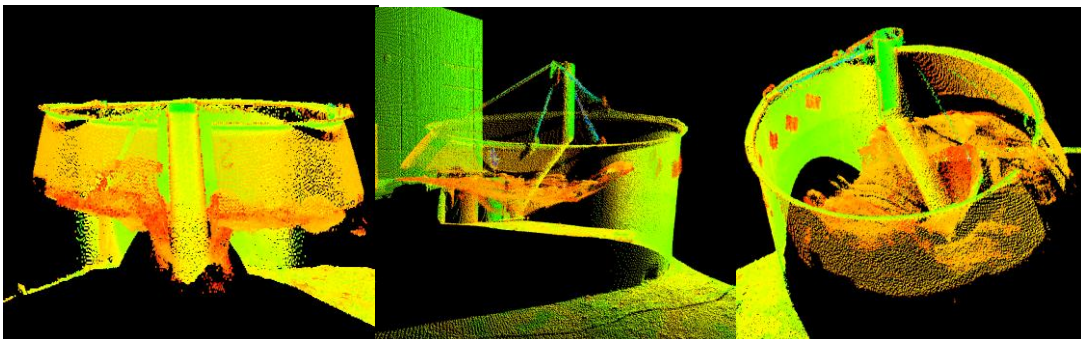
Figure 74: Refracted 3D Images of Stations I, II, and III.

The refracted point clouds from each station were extracted from their positions and copied into a new modelspace view. The extracted point clouds were exported from Cyclone as a text file and were imported into MATLAB. The water refraction correction code was applied in MATLAB to align the refracted point clouds into their proper positions. The results of the refraction correction plots are shown in Figures 75.1 (a) through 75.3 (c).
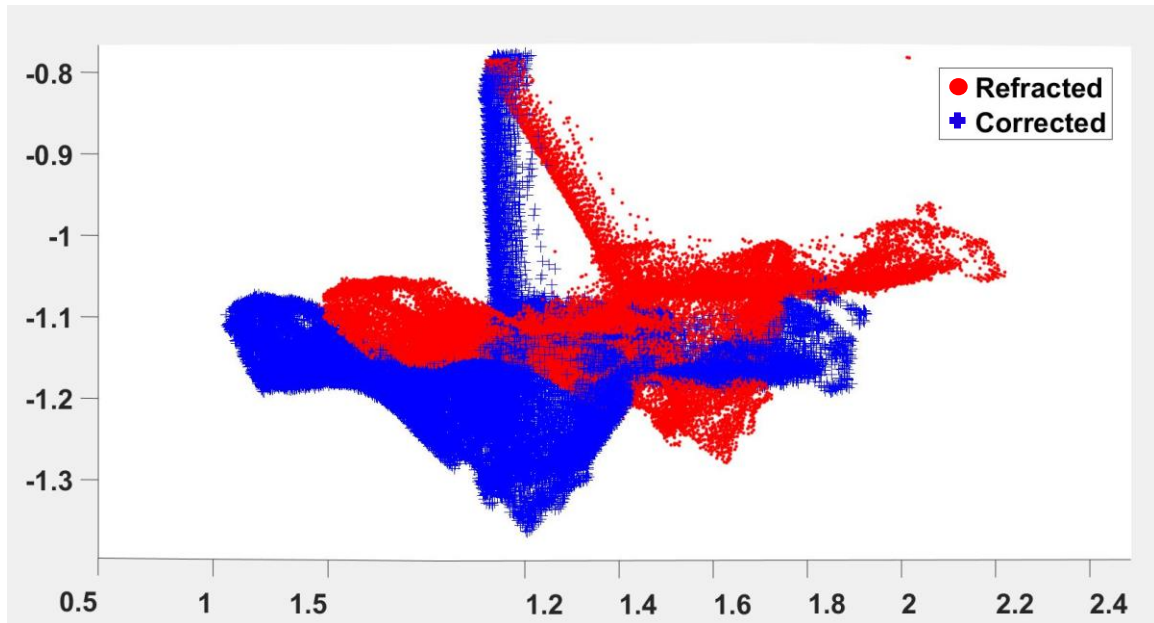
Figure 75.1 (a): Refracted and Corrected Point Clouds of Station I
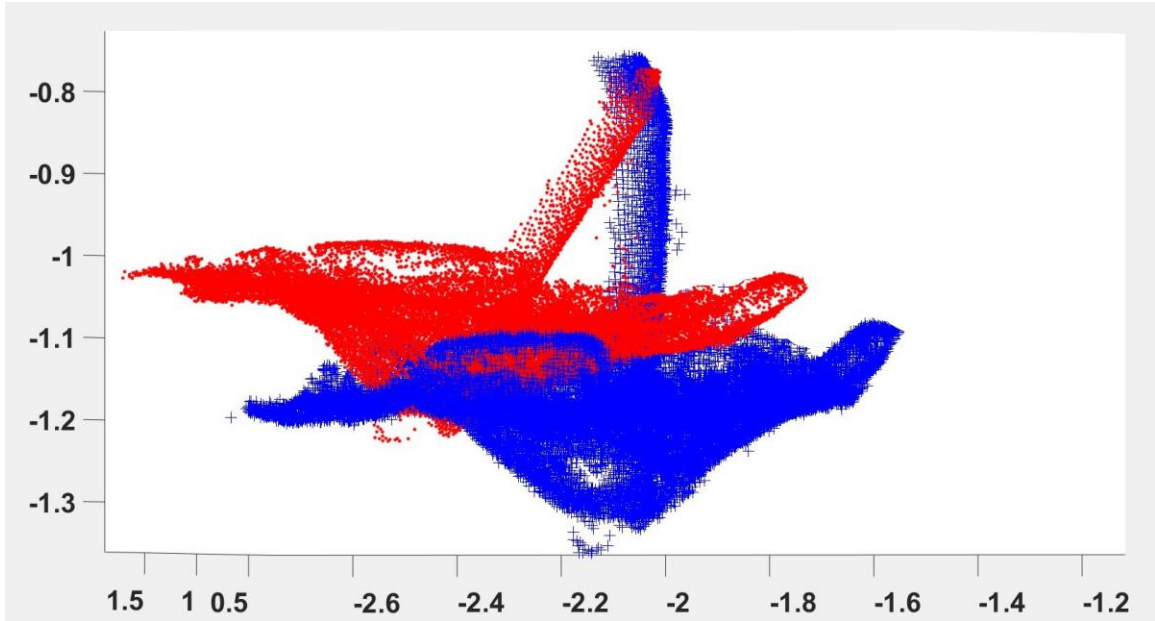
Figure 75.2 (b): Refracted and Corrected Point Clouds of Station II
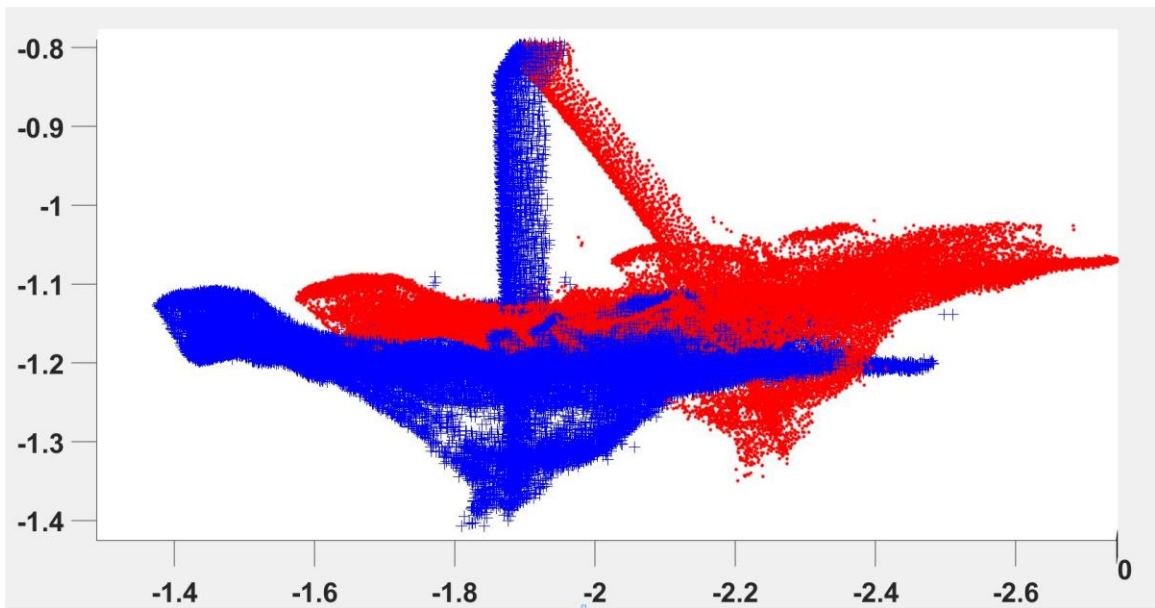
Figure 76.3 (c): Refracted and Corrected Point Clouds of Station III

The subsequent plots shown in Figures 75.1 (a) through 75.3 (c) display the refracted point clouds in red dots and the corrected point clouds in blue x marks. The red-

dotted refracted points appeared to be slanted from the surface of the water to the bottom of the scour hole. The blue-dotted corrected points appeared to be in a vertical position, which is the correct alignment of the bridge pier and scour hole model. After running the analysis in MATLAB, the corrected text files were imported into Cyclone, and the corrected point clouds were properly aligned into their original positions. The corrected 3D images are shown in Figure 76.

Station I   **Station II**

Station III
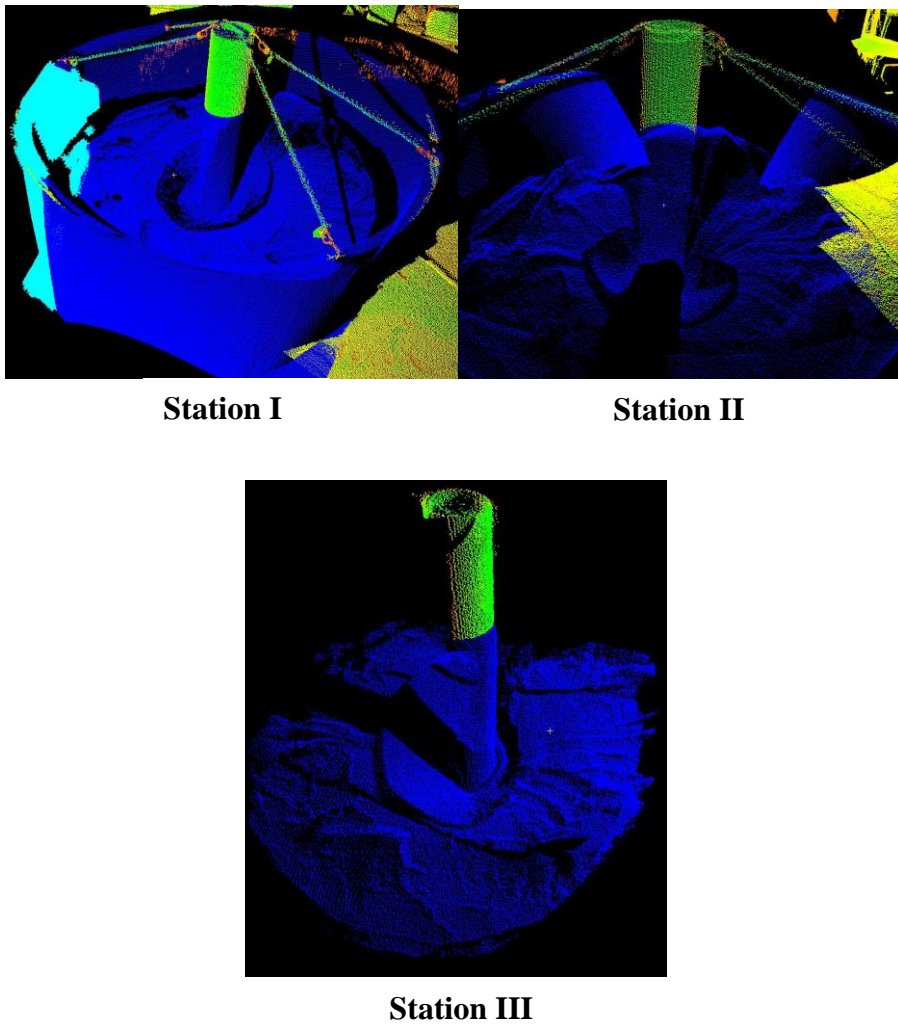
Figure 77: Corrected 3D Images of Stations I, II & III

After importing the corrected point clouds into Cyclone, the target-based registration was conducted between stations I, II and III. The cloud-constraint wizard was utilized to select overlapping points in stations I and II. The points in station I were dotted on various point clouds around the test tank and overlapped with the points in station II. The points in station I that corresponded with the points in station II had matching coordinates and elevations. The points must overlap with each other so as not to cause a distortion in the image during the registration process. The dimensions of the final image of the registered simulated scour hole is shown isometrically in Figure 77.
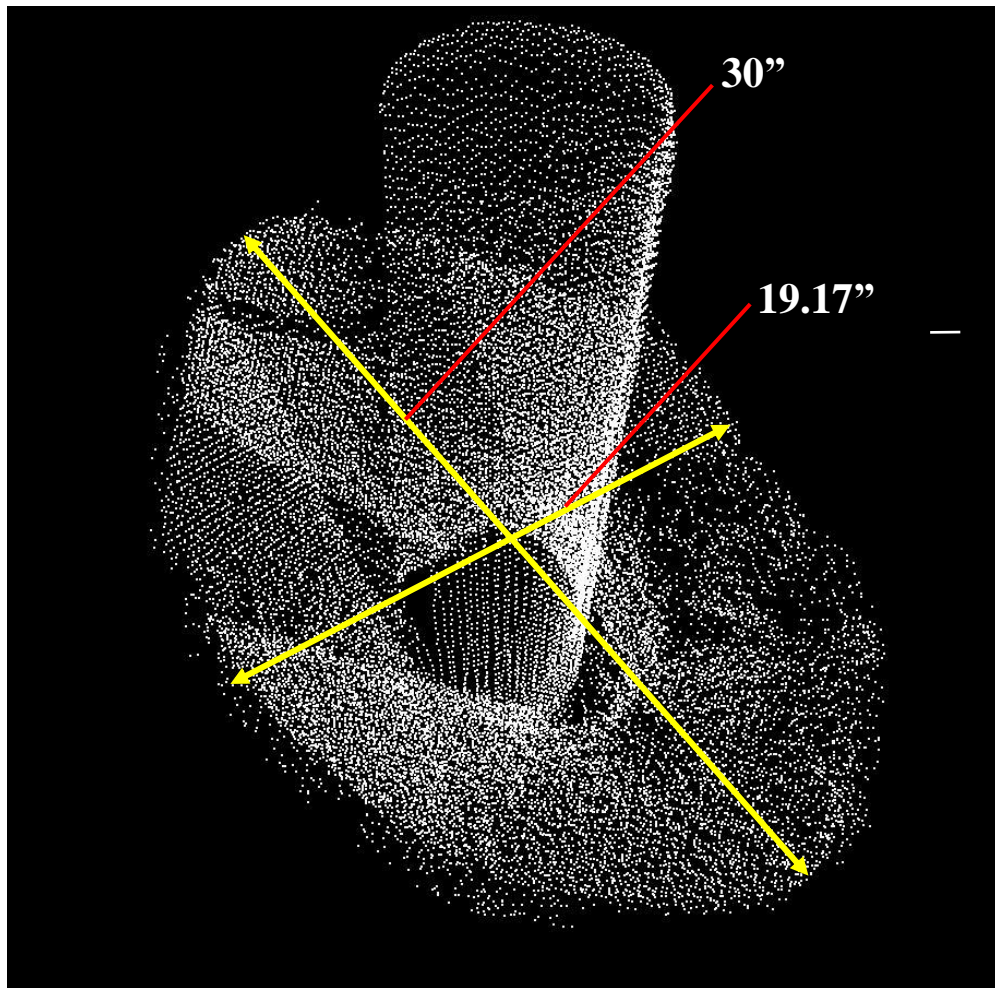
Figure 78: Registered Simulated Scour Hole
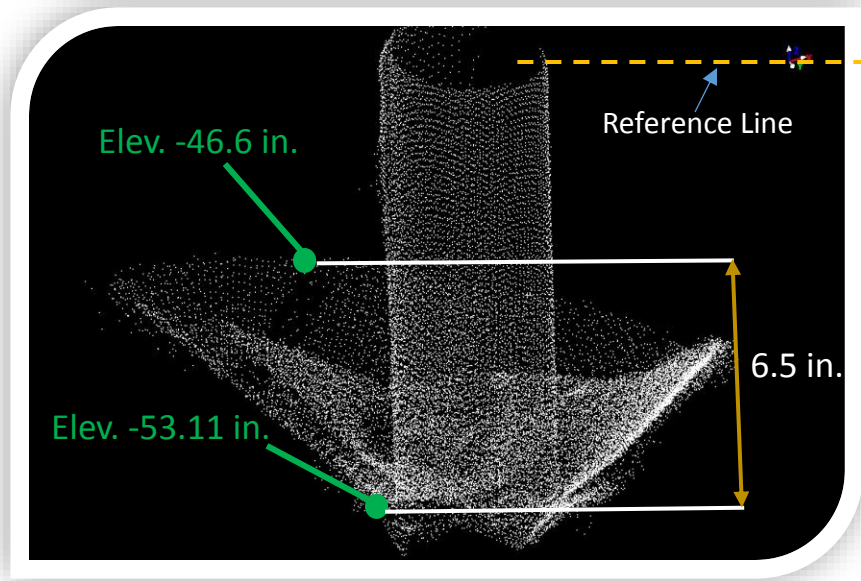
Figure 78: Elevation View of Registered Scour Hole

The elevations of the scour hole profile after applying water refraction correction is

shown in Figure 78. The elevation at the top of the scour hole was -46.6 inches from the

reference line dashed in orange, and -53.11 inches at the bottom surface of the scour hole.

The elevation points were identical to the elevation points of the dry scour hole.

4.2 SCOUR MEASURMENT USING HYDROLITE SONAR

The HydroLite Sonar instrument was utilized to log elevation points along the water

surface from eight different segments. Each segment had a starting point at the outermost

curvature of the test tank and an endpoint at the surface of the cylindrical bridge pier model.

The elevation points of the scour model were transmitted from the Echosounder to the data

collector via Bluetooth. The survey data in the collector unit has indicated that the height

of the GPS unit was 6 feet from the transducer. The elevation points that were logged into

the data collector were known as "Point ID" and each point has a different point ID number, depending upon the order.

4.2.1 CASE STUDIES I & II

Case Study I was based on the measurement of the maximum depth of the 8.5-inch scour model. The scour model (with known dimensions) has a steep slope from all directions and a maximum depth of 8.5 inches. The HydroLite Sonar was used to take measurements of the scour model to compare the measured shape with the real shape.

The hydrographic survey points were imported from the data collector to the PC as ASCII points and were in the X,Y,Z format. The X-coordinate represented the eastward-measured distance of the point, the Y-coordinate represented the elevation of the point, and the Z-coordinate represented the northward-measured distance of the point. The X,Y,Z data were comma-delimited on Microsoft Excel and then were imported into MATLAB Software. A code analysis was applied in MATLAB to program the X,Y,Z data to plot a 3D-Mesh of the hydrographic survey points. Figure 78 illustrates a 2D graph of the survey points that were taken along the eight segments. Figure 79 shows a 3D plot of the hydrographic survey points along the slopes of the local scour hole. The transducer began logging survey points at an elevation of 12 inches (water surface elevation). The transducer pulse reached the bottom surface of the scour hole at an elevation of 20.5 inches. This indicated that the maximum depth of the scour hole was 8.5 inches. Figures 80 through 81 show the 3D triangulation meshes for the 8.5-inch and 6.5-inch scour holes respectively. In Figure 81, the maximum depth of the scour hole is 6.5 inches.
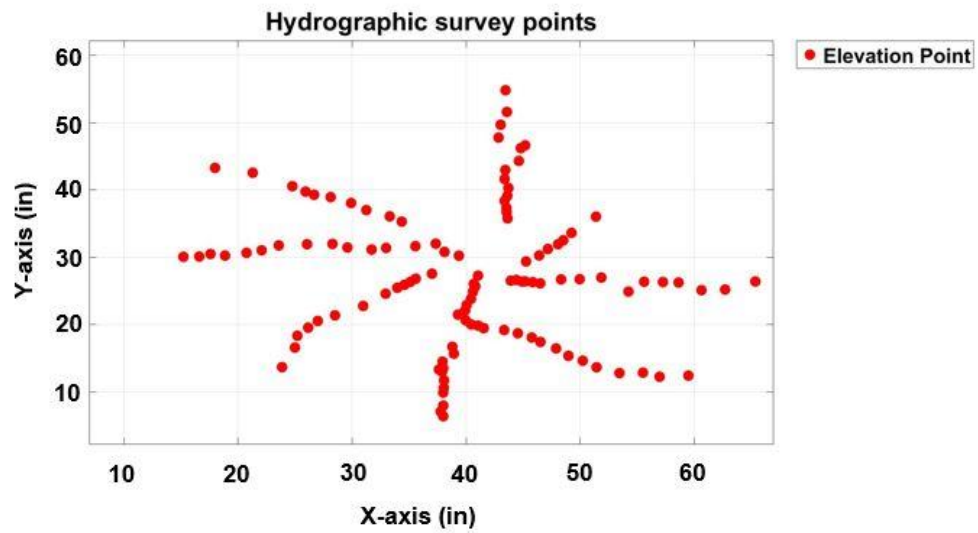
Figure 79: 2D graph of Survey Points Along Sonar Pathway
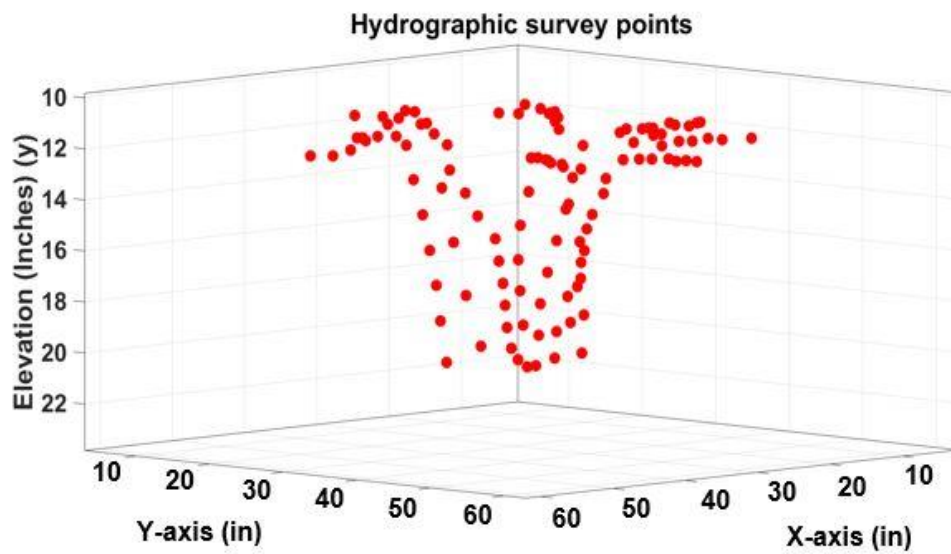
Figure 80: Hydrographic Survey points of 8.5-Inch Scour Hole
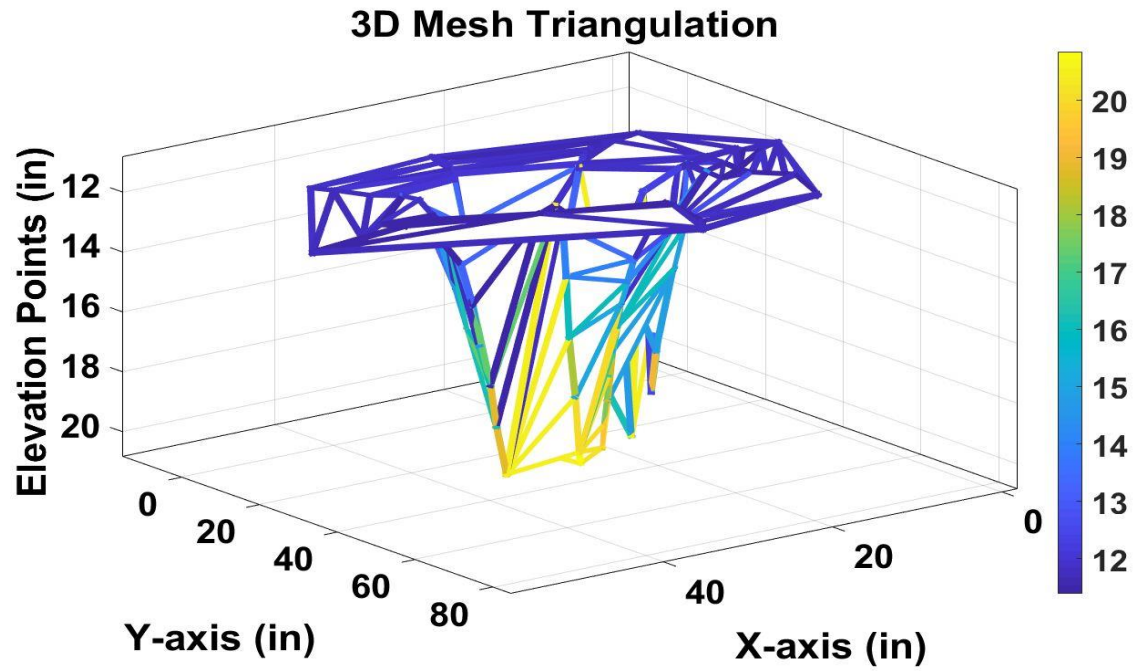
Figure 81: 3D-Mesh Triangulation of 8.5" Scour Hole
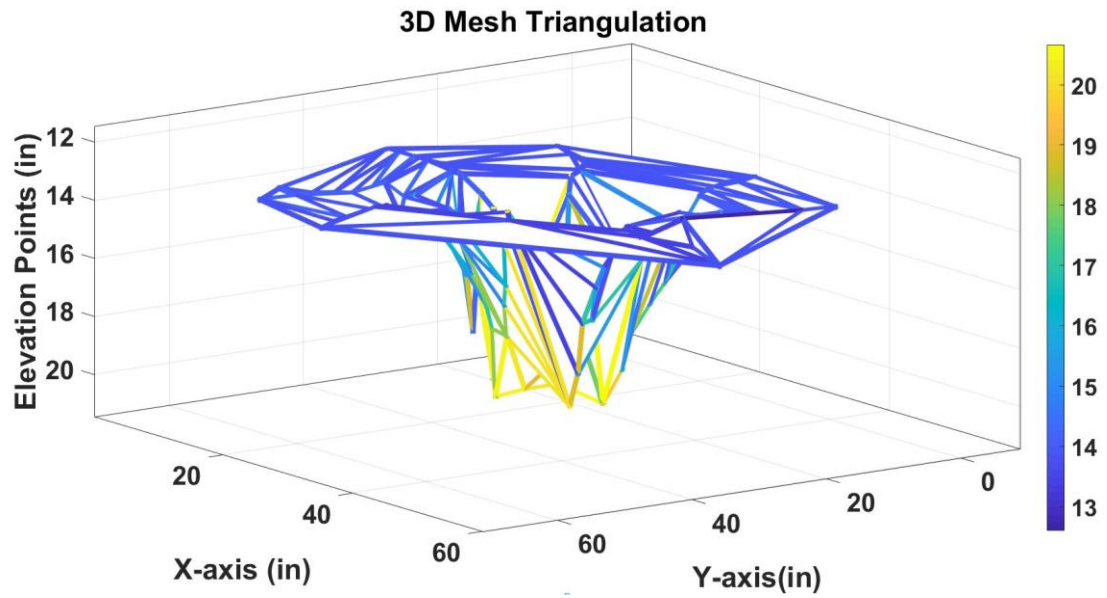
Figure 82: 3D-Mesh Triangulation of 6.5" Scour Hole

4.3 COMPARISON OF GREEN LASER BASED METHOD WITH HYDROLITE SONAR TECHNIQUE

The Green Laser and HydroLite Sonar instruments both have complimentary features for scour monitoring and underwater inspection. The green laser can travel through multiple mediums and make several interactions with the surface, whereas the HydroLite Sonar can only collect readings via sound pulse through the water column, and not through air. The green laser traveled from the air medium and penetrated through the water surface, which caused a refraction on its refraction plane and reached the streambed of the water column. The Sonar was able to record elevation points of the streambed from the water surface without refraction. The sonar rod was fixed in a vertical position over the water, and the transducer emanated a sound pulse that was used to assess the geometry of the scour hole, where high levels of detail were not required.

The Green Laser method provided several advantages over the HydroLite Sonar. The measurement resolution in green laser had multiple orders of higher magnitude, enabling very dense point clouds of the scanned scour hole. The measurements made from millions of highly dense point clouds were more accurate than those taken from the hydrographic survey of the sonar. The sonar displayed discrete elevation points of the sloped scour hole, which showed the maximum scour depth but did not provide the full 3D image of the scour's geometrical shape. The Green Laser beam was capable of capturing the edges of the scour hole much more precisely than the sonar instrument. Unlike the Green Laser, the sonar's beam width was 4 degrees which may have caused two sonar pulses to have overlapping footprints, which may lead to inaccurate measurements (2G Robotics, http://www.2grobotics.com/wp-content/uploads/2017/03/sonarvslaser.pdf).

CHAPTER 5: CONCLUSIONS AND RECOMMENDATIONS

5.1 CONCLUSIONS

This research has demonstrated a feasible, non-intrusive and non-contact methodology for scour monitoring and mapping that is less laborious and less expensive as compared to traditional visual inspections. As the laser scanning technique collects thousands of samples on the scour in minutes, it can produce a detailed shape of the scour hole, which is crucial to model and predict the future threats to the structural stability of bridge structures. The simulation of model clear water bridge pier scour hole was based on published dimensionless analysis for scour hole characteristics.

By utilizing the demonstrated optical laser-based 3-D scanning, the refraction correction process allowed for the 3-D model of the scour hole to be reconstructed. After conducting the refraction correction in Case I, the scour model was compared with the original scour setup under dry condition, and the mean distance error was 27 mm. Despite being high, the relative shape of the scour models before and after filling with water, is fairly identical where both baseline (before filling with water) and corrected (after filling with water) scour models were within 1% consistent with the design dimensions. As for Case II, the water refraction correction was applied on all three stations and the final registered image displayed a maximum depth of 6.5 inches, which is equivalent to the depth of the original scour hole model.

For Cases I and II under dry conditions, the green laser scanned the test-tank region from three stations, a co-registration was applied to combine all of the three overlapping scans into one complete 3D image. In Case I, it was concluded that 1.1 inches below the bottom surface of the simulated scour hole was captured. In addition, the width and length of baseline condition was within 1% of design dimensions. In Case II, the elevation points from the top surface to the bottom surface of the scour indicated that the maximum depth (6.5 inches) was equivalent to the depth of the original scour model. The measured longitudinal and transverse dimensions were equivalent to the dimensions of the original scour model as well.

5.2 APPLICATION OF GREEN LASER IN REAL LIFE SITUATIONS

The Green Laser scanner was used in a laboratory experiment to measure the depth of simulated scour holes around a bridge pier model under both dry and clear water conditions. Based on this laboratory analysis, the results suggest that this non-contact instrument has the potential for scour mapping and monitoring around bridge piers. Unlike the existing scour monitoring devices, the green laser is feasible in the sense that it can collect millions of highly dense point clouds of the streambed's topography in a matter of minutes. This procedure can be done by a bridge inspector. The scanner can be temporarily mounted over the pier at the edge-wall of the bridge deck and conduct a scanning session. The same procedure is repeated at the corresponding edge-wall to scan the other region of the pier, then co-registering both scanning sessions to combine them into one whole scan of the 3D image around the pier. This technique is used for detecting potential local scour around bridge piers. The HydroLite Sonar can be used for scour mapping to detect potential large scour around the entire bridge.

5.3 RECOMMENDATIONS AND FUTURE RESEARCH WORK

- The future research will analyze the factors that affect the accuracy of the refraction correction, such as turbidity and water flow.

- Additional analysis is needed for various submerged materials that influence the refractive index and systematic errors in the equipment. Due to the direct sunshine and high reflective materials in and around the experimental setup, the existence of noise was high.

- Though the noise was manually removed in this work, the future research will use statistical methods to eliminate them automatically.

- The relation between the turbidity and transmissivity/reflectivity of the water will also be studied in the future to reflect real-world scenario.

- The present study can be continued to take into account the effect of water turbidity levels, specific conductance (freshwater or salt water), and temperature.

- The other common scour scenarios can also be studied using green laser based monitoring and mapping technique in the future.

- Further research could focus on the use of HydroLite Sonar in real world situations to conduct hydrographic surveys in large-scale areas around bridge piers under various water depths and flow velocities.   (

REFERENCES

(1) National Bridge Inventory Data 2015, https://www.fhwa.dot.gov/bridge/nbi/ascii.cfm, Accessed on 07/20/2017

(2) Brice JC, Blodgett JC. Countermeasures for hydraulic problems at bridges, Vol.1&2, FHWA/RD-78-162&163, Federal Highway Administration, U.S. Washington, D.C.: Department of Transportation; 1978.

(3) N.T.S.B. Collapse of New York Thruway (I-90) Bridge, Schoharie Creek, Near Amsterdam, New York, April 5, 1987, NTSB number: HAR-88/02, NTIS number: PB88-916202; 1987.

(4) N.T.S.B. Collapse of the Northbound U.S. Route 51 Bridge spans over the Hatchie River, Near Covington, Tennessee, April 1, 1989, NTSB number: HAR- 90/01, NTIS number: PB90-916201; 1987.

(5) Prendergast, L. J., & Gavin, K. (2014). A review of bridge scour monitoring techniques. Journal of Rock Mechanics and Geotechnical Engineering, 6(2), 138-149.

(6) Arneson, L. A., Zevenbergen, L. W., Lagasse, P. F., & Clopper, P. E. (2012). Evaluating scour at bridges. Hydraulic Engineering Circular No. 18, Publication No. FHWA-HIF-12-003, Fifth Edition, April 2012

(7) Lagasse, P. F., Zevenbergen, L. W., Spitz, W. J., & Arneson, L. A. (2012). Stream stability at highway structures, Hydraulic Engineering Circular No. 20, Publication No. FHWA-HIF-12-004, Fourth Edition, April 2012

(8) Lagasse, P. F., Clopper, P. E., Pagan-Ortiz, J. E., Zevenbergen, L. W., Arneson, L. A., Schall, J. D., & Girard, L. G. (2009). Bridge Scour and Stream InstabilityCountermeasures: Experience, Selection and Design Guidance. Volume 1, Hydraulic Engineering Circular No. 23, Publication No. FHWA-NHI-09-111, Third Edition, September 2009

(9) Hunt, B. E. 2005. Practices for Monitoring Scour Critical Bridges. 2005. NCHRP Project 20-5 first draft report, Transportation Research Board, National Research Council, National Academy Press, Washington, D.C.

(10) ASCE 2017 Infrastructure Report Card, Bridges, https://www.infrastructurereportcard.org/wp-content/uploads/2017/01/Bridges-Final.pdf, Accessed on 07/20/2017

(11) Fisher, M., Chowdhury, M. N., Khan, A. A., & Atamturktur, S. (2013). An evaluation of scour measurement devices. Flow Measurement and Instrumentation, Volume 33, 2013, Pages 55-67

(12) Briaud, J. L., Hurlebaus, S., Chang, K. A., Yao, C., Sharma, H., Yu, O. Y., & Price, G. R. (2011). Realtime monitoring of bridge scour using remote monitoring technology. Austin, TX., https://static.tti.tamu.edu/tti.tamu.edu/documents/0-6060-1.pdf, Accessed on 07/20/2017

(13) Elsaid, A. H., (2011), Vibration Based Damage Detection of Scour in Coastal Bridges. Doctoral dissertation, North Carolina State University, Raleigh, NC 27695

(14) Forde, M. C., McCann, D. M., Clark, M. R., Broughton, K. J., Fenning, P. J., & Brown, A. (1999). Radar measurement of bridge scour. Ndt & E International, 32(8), 481-492.

(15) De Falco, F., & Mele, R. (2002). The monitoring of bridges for scour by sonar and sedimetri. NDT & E International, 35(2), 117-123.

(16) Multibeam Sonar theory of operation, L-3 Communications SeaBeam Instruments, https://www.ldeo.columbia.edu/res/pi/MB-System/sonarfunction/SeaBeamMultibeamTheoryOperation.pdf, Accessed on 07/20/2017

(17) Umeda, S., Yamazaki, T., & Yuhi, M. (2010). An experimental study of scour process and sediment transport around a bridge pier with foundation. In proceedings of International Conference on Scour and Erosion (ICSE-5) Scour and Erosion (pp. 66-75).

(18) Rieke-Zapp, D. H. and Nearing, M. A. (2005), Digital close-range photogrammetry for measurement of soil erosion. The Photogrammetric Record, 20: 69–87

(19) Heng, B.C.P., Chandler, J.H. and Armstrong, A., 2010. Applying close range digital photogrammetry in soil erosion studies. The Photogrammetric Record, 25 (131), pp. 240-265.

(20) Smith, M., Vericat, D., & Gibbins, C. (2012). Through-water terrestrial laser scanning of gravel beds at the patch scale. Earth Surface Processes and Landforms, 37(4), 411-421.

(21) Plenner, S. (2014). Development and application of a simple terrestrial laser scanner. Master thesis report, The University of Iowa. Iowa City, IA

(22) Hodge, R., Brasington, J. and Richards, K. (2009), In situ characterization of grain-scale fluvial morphology using Terrestrial Laser Scanning. Earth Surf. Process. Landforms, 34: 954–968

(23) Miura, N., & Asano, Y. (2013). Green-wavelength terrestrial laser scanning of mountain channel. ISPRS Annals of Photogrammetry, Remote Sensing and Spatial Information Sciences, (2), 187-192.

(24) Daimon M, Masumura A. 2007. Measurement of the refractive index of distilled water from the near-infrared region to the ultraviolet region. Applied Optics 46: 3811–3820

(25) Ettema,R., Constantinescu,G., and Melville, B., Evaluation of Bridge Scour Research: Pier Scour Processes and Predictions, 2011, NCHRP Project 24-27(01)

(26) Richardson, E. V. and Davis, S. R. "Evaluating scour at bridges," 2001, Fourth Edition. Federal Highway Administration, Washington D.C

(27) Richardson, E.V., Briaud, J.L., and Buchanan,S.J., Praktische Berechnungen zu Kolken an Brücken in den USA United States Practice for Bridge Scour Analysis, 2002, Mitteilungsblatt der Bundesanstalt für Wasserbau Nr. 85 (2002)

(28) Khwairakpam, P., Ray, S. S., Das, S., Das, R., and Mazumdar, A., Scour Hole Characteristics Around a Vertical Pier Under Clearwater Scour Conditions, 2012, ARPN Journal of Engineering and Applied Sciences ISSN 1819-6608, Vol.7, No.6, June 2012

(29) CloudCompare Software manual, http://www.danielgm.net/cc/doc/qCC/CloudCompare%20v2.6.1%20-%20User%20manual.pdf, Accessed on 07/20/2017

(30) Leica Cyclone. (n.d.). Retrieved November 08, 2017, from http://hds.leica-geosystems.com/en/Leica-Cyclone_6515.html

(31) Prendergast, L.J., and K. Gavin. "A review of bridge scour monitoring techniques." Journal of Rock Mechanics and Geotechnical Engineering, Elsevier, 3 Feb. 2014

(32) S. Nagarajan, M. Arockiasamy, and M. Banyhany, "Bridge Pier Scour Hole

Simulation and 3D Reconstruction Using Green Laser", 97th Annual Meeting of the

Transportation Research Board, Washington, Jan. 7-11, 2018

(33) 2G Robotics Underwater Laser Scanners. "Documentation." *Sonar vs. Laser,*

https://www.mathworks.com/help/matlab/software-development.html